ERK and PKA signaling drive the evolutionary expansion of the cortex

Zhuangzhi Zhang[1]†, Zhejun Xu[1]†, Tongye Fu[1]†, Jialin Li†, Feihong Yang[1], Chuannan Yang[1], Wenhui Zheng[1], Zizhuo Sha[1], Yanjing Gao[1], Mengge Sun[1], Zhenmeiyu Li[1], Jing Ding[1], Xiaosu Li[1], Zhengang Yang*[1]

†These authors contributed equally to this work

[1]State Key Laboratory of Medical Neurobiology and MOE Frontiers Center for Brain Science, Institutes of Brain Science, and Department of Neurology, Zhongshan Hospital, Fudan University, Shanghai 200032, China

*Zhengang Yang: yangz@fudan.edu.cn

Abstract

The cerebral cortex, the anatomical foundation of human intelligence, underpins our advanced cognition and language. Deciphering the regulatory mechanisms driving its expansion in neuronal number and surface area is essential for elucidating the unique features of the human brain. Here, we demonstrate that ERK and PKA signaling pathways coordinately maintain the neurogenic identity and lineage specification of cortical radial glia (RGs) by suppressing gliogenic YAP and SHH signaling. Conversely, YAP signaling promotes the RG-ependymal glial cell lineage by inhibiting ERK, PKA, and SHH signaling, while SHH signaling facilitates the generation of cortical tripotential intermediate progenitor cells (Tri-IPCs) from RGs by repressing ERK, PKA, and YAP signaling. Cortical Tri-IPCs exhibit a sequential differentiation potential, giving rise to cortical astrocytes, oligodendrocytes, and olfactory bulb interneurons. Importantly, we provide compelling evidence for the evolutionary conservation of these molecular mechanisms between mice and humans. Thus, ERK and PKA signaling in cortical RGs establish a mutually reinforcing positive feedback loop, mediated through repressing gliogenic YAP and SHH signaling, which collectively promote RG proliferation, protect neurogenesis, and drive human cortical expansion. This study identifies a unifying principle governing cortical neurogenesis, gliogenesis, expansion, and evolution.

Keywords: cortical development, ERK, PKA, YAP, SHH signaling,

Introduction

Radial glial (RGs), spanning the entire thickness of the developing cortex, are primary neural stem cells [1-6]. During mouse corticogenesis, three distinct types of RGs can be classified based on their cell lineage, which we designate as N-RGs, E-RGs, and T-RGs. The early RGs are neurogenic (N-RGs), generating intermediate progenitor cells (IPCs) exclusively for glutamatergic pyramidal neurons (PyN), known as PyN-IPCs [1-6]. At the end of cortical neurogenesis, a subpopulation of N-RGs transform into E-RGs that generate ependymal-IPCs (EP-IPCs), which produce ependymal cells [7]. Meanwhile, another population of N-RGs transform into T-RGs, generating tripotential intermediate progenitors (Tri-IPCs) that express ASCL1, EGFR, and OLIG2. These Tri-IPCs sequentially generate cortical astrocyte lineage-restricted IPCs (APCs), oligodendrocyte lineage-restricted IPCs (OPCs), and IPCs for cortically derived olfactory bulb interneurons (OBIN-IPCs). These lineage-restricted IPCs then divide symmetrically to generate cortical astrocytes, oligodendrocytes, and OBINs, respectively [8-13].

During human corticogenesis, full-span radial glial cells (fRGs) persist from gestational week (GW) 8 through GW16. Around GW16, fRGs give rise to the truncated radial glia (tRGs) in the ventricular zone (VZ) and the outer radial glia (oRGs, also known as basal RGs) in the outer subventricular zone (outer SVZ, OSVZ) [13,14]. Human cortical fRGs are neurogenic, mainly generating PyN-IPCs for deep layer PyNs. Human cortical oRGs, which are rare in mice, are also neurogenic, mainly generating PyN-IPCs for upper layer PyNs [4,10,12,13,15].

Similar to mouse cortical RGs, human tRGs exhibit three distinct subtypes, referred to as N-tRGs, E-tRGs, and T-tRGs. After human fRGs generate N-tRGs, they start to express EGFR and ASCL1, but initially generate PyN-IPCs for upper layer PyNs (GW16-GW17) [9,13]. Around GW18, N-tRGs transition from neurogenesis to gliogenesis. A subset of N-tRGs become E-tRGs, which generate cortical EP-IPCs [9,10,13,16]. In parallel, another population of N-tRGs becomes T-tRGs, giving rise to Tri-IPCs [9,10,13,15].

Here, we have explored the mechanisms underlying the lineage progression of cortical RGs. We demonstrate that four evolutionarily ancient signaling pathways, ERK, PKA, YAP, and SHH are essential for regulating the identity and lineage specification of distinct cortical RG subtypes in mouse and human. Together our data reveal a unifying principle underlying cortical development and evolution.

Results

Molecular identity of human cortical oRGs, E-tRGs, and T-tRGs

In contrast to the mouse, human cortical development is more protracted and has more RG/progenitor types. To identify the molecular features of human cortical oRGs, E-tRGs, and T-tRGs, we reanalyzed published scRNA-Seq data using the human GW22 cortical tissue [17]. The heatmap presents a comprehensive profile of 28 genes (Fig. 1a, b), illustrating the molecular identity and potential cell lineage relationships among human cortical oRGs, E-tRGs, and T-tRGs (Fig. 1c-f). Our analysis revealed that all pathways suppress SHH and YAP signaling (YAP/TAZ activity) in human cortical oRGs.

ERK signaling is activated by the binding of FGFs to FGFRs [12,18]. While FGF2 and FGFR1/2/3 are expressed at comparable levels in human cortical oRGs, E-tRGs, and T-tRGs, ERK signaling intensity varies, being strongest in oRGs, weakest in E-tRGs, and intermediate in T-tRGs (Fig. 1b). This conclusion is based on the expression levels of ERK signaling response genes, including *BMP7, ETV1, ETV5, HOPX*, and *SPRY2* (Fig. 1b; Extended Data Fig. 1a, b). Moreover, we observed that cAMP-PKA signaling activity exhibits a pattern similar to that of ERK signaling across RGs. For example, G protein-coupled receptor genes *ADCYAP1R1* and *ADORA2B* are expressed much higher in oRGs than E-tRGs and T-tRGs (Fig. 1b; Extended Data Fig. 1b). ADCYAP1R1 binds to PyN-derived ADCYAP1, resulting in the activation of the coupled GNAS (Gsα) to stimulate adenylyl cyclase activity to increase cAMP-PKA signaling [19]. Likewise, adenosine binding to ADORA2B also activates cAMP-PKA signaling [20]. cAMP-PKA-CREB targets include *DIO2* (Kohrle and Fradrich, 2022) and *CXCL14* [21]. The *DIO2* promoter in humans, rats, and mice contain a conserved canonical cAMP response element [22]. Accordingly, we observed that oRGs expressed higher levels of *DIO2* and *CXCL14* compared with E-tRGs and T-tRGs (Fig. 1b; Extended Data Fig. 2b), providing evidence that oRGs have high PKA activity.

PKA-mediated phosphorylation of FGF2 increases its binding affinity up to 8-fold and potentiates ERK activity [23]. Moreover, ERK and PKA signaling can mutually reinforce each other [24,25]. PKA represses SHH-SMO and YAP signaling [26-28]. Taken together, this analysis demonstrates that heightened ERK and PKA activity represents a defining feature of human cortical oRGs.

A prominent feature of human cortical E-tRGs is the robust activation of YAP signaling. YAP signaling is required for cortical ependymal cell formation [29,30]. YAP signaling signature genes are highly expressed in E-tRGs, including, *CCN1 (CYR61), CCN2 (CTGF), AMOTL2, WWC1*, and *WWTR1 (TAZ)* (Fig. 1b; Extended Data Fig. 1c). Consequently, markers for early ependymal cells, including *ANXA2, CRYAB, FOXJ1*, and *GMNC*, are also expressed in E-tRGs (Fig. 1b; Extended Data Fig. 1c).

Furthermore, CXCL12/CXCR signaling is upregulated in E-tRGs compared to oRGs and T-tRGs (Fig. 1b; Extended Data Fig. 1c), which represses cAMP-PKA signaling [27]. Indeed, PKA and ERK signaling are extremely low in E-tRGs (Fig. 1b). This observation aligns with previous studies demonstrating a reciprocal regulatory relationship between these pathways: while PKA activity inhibits YAP signaling [27,28], YAP signaling conversely suppresses both cAMP-PKA and ERK signaling [31,32]. Furthermore, YAP signaling inhibits primary cilium assembly [33], which may suppress SHH-SMO signaling. Collectively, this analysis provides evidence that YAP signaling, by repression of PKA, ERK, and SHH signaling, is a key feature of E-tRGs.

At GW22, T-tRGs exhibit low to moderate levels of ERK, PKA, YAP, and SHH signaling (Fig. 1b; Extended Data Fig. 1a-d), indicating the convergence of multiple signaling pathways. Indeed, *EGFR* and *ASCL*, which are activated by ERK, SHH and/or YAP signaling, are expressed by a subpopulation of T-tRGs [10,13,15,34]. These T-tRGs give rise to Tri-IPCs that subsequently generate APCs, OPCs and OBIN-IPCs [4,9,10,13,15]. However, at GW22, we identified APCs and OPCs, but not OBIN-IPCs, derived from Tri-IPCs (Extended Data Fig. 2a-f). With increased SHH signaling at GW23 and GW26 there was increased expression of *GLI1* and *HHIP* in T-tRGs and their progenies. Furthermore, genes of OBIN-IPCs, including *GSX2*, *DLX2*, *GAD2*, and *SP9*, became evident within the Tri-IPC cluster (Extended Data Fig. 3a-g). SHH-SMO signaling represses PKA signaling [26,27]. The SHH-SMO signaling may additionally suppress ERK signaling through the activation of PP2A-mediated mechanisms [35,36]. Studies also suggested that the functional interplay between YAP and SHH signaling governs the specification of different cell types [37]. As observed in the cortex, YAP signaling drives the cortical E-tRG-derived multiciliated ependymal cell lineage [29,30], whereas SHH-SMO signaling promotes the primary-ciliated T-tRG-derived Tri-IPC cell lineage [8,10,12,15].

In summary, during the later stages of human cortical development, PyN-IPC-generating oRGs, ependymal-IPC-generating E-tRGs, and Tri-IPC-generating T-tRGs develop distinct molecular signatures, driven by different conserved signaling pathways that mutually inhibit one another (Fig. 1c-f). This indicates that the sustained neurogenic capacity of human oRGs, a fundamental driver of cortical neurogenesis and expansion, is regulated through the combined action of ERK and PKA signaling that coordinately suppress gliogenic YAP and SHH signaling activities. To experimentally validate these mechanistic insights, we employed complementary mouse genetic approaches.

YAP signaling controls cortical E-RG identity

Increased nuclear translocation of YAP/TAZ proteins in mouse cortical RGs from E12.5 to E16.5, enhances YAP signaling which correlates with advancing stages of cortical development [29,30]. To investigate the role of YAP signaling in cortical RGs, we crossed mice harboring a *WWC*-derived floxed minigene (referred to as *SuperHippo*)

with *hGFAP-Cre* mice. *SuperHippo* specifically inhibits YAP signaling, mimicking *Yap1/Wwtr1* double knockouts (Fig. 2a) [38]. To label E15.5 progenitors, we injected FlashTag into the lateral ventricle of littermate wild type control *and hGFAP-Cre; SuperHippo* mice. At E16.5, we isolated FlashTag-labeled cortical cells for scRNA-Seq analysis. Blocking YAP signaling reduced expression of *Cyr61, Ctgf, Amotl2*, and *Wwc2* in cortical RGs (Extended Data Fig. 4a-c), and eliminated expression of *Cryab* and *Foxj1 (*early ependymal cell markers) (Extended Data Fig. 4c). On the other hand, ERK signaling response genes (e.g. *Etv1, Etv5, Spred1/2, Spry2, Bmp7, Id1/3,* and *Hopx)* were upregulated (Extended Data Fig. 4c). *Gnas*, a signature PKA signaling gene, was also increased, suggesting that a subpopulation of cortical RGs in *hGFAP-Cre; SuperHippo* mice exhibit molecular features of human oRGs, based on their higher ERK and PKA signaling.

The *hGFAP-Cre; SuperHippo* mutant had increased SHH-SMO signaling based in upregulation of *Gas1, Gli1, Gli2, Gli3, Hhip, Ptch1,* and *Smo* (Extended Data Fig. 4c), suggesting that a subpopulation of cortical RGs in *hGFAP-Cre; SuperHippo* mice had molecular features of T-RGs. ERK signaling enhances self-renewal of cortical RGs [12], while SHH-SMO signaling promotes the generation of Tri-IPCs from cortical RGs [8,10]. Correspondingly, expression of PyN-IPC marker genes *Eomes* (*Tbr2*) and *Neurog2* was downregulated in the mutant RGs (Extended Data Fig. 4c). These findings were further validated through scRNA-Seq analysis of *Emx1-Cre; SuperHippo* mice at E16.5 (Extended Data Fig. 5a, b).

By P2, E-RGs and their progeny ependymal cells were lost in *hGFAP-Cre; SuperHippo* mice (Fig. 2b, c; Extended Data Fig. 6a, b), consistent with previous studies [29,30]. Immunohistochemical analysis demonstrated an increase in Tri-IPCs and the loss of ependymal cells (Fig. 2d, Extended Data Fig. 4d, e; Extended Data Fig. 5c-e). In the T-RGs, YAP-signaling genes were downregulation, and the expression of *Cryab, Foxj1*, and *Ogn* (ependymal markers), was abolished (Fig. 2c; Extended Data Fig. 6b). In contrast, ERK, PKA, and SHH signaling were upregulated (Fig. 2c; Extended Data Fig. 6b).

Finally, we reanalyzed bulk RNA-Seq and ChIP-Seq data from mice expressing the YAP1-MAMLD1 (YAP-M) fusion protein, which is implicated in supratentorial ependymoma [34]. The gene expression profiles demonstrated distinct patterns between cells from the SVZ of wild-type control mice (n=3) and tumor cells derived from ~P20 mice transfected with *YAP-M* at E14.5 (n=4) [39]. The *YAP-M* fusion oncogene significantly upregulated expression of YAP signaling components and early ependymal cell markers, while mature ependymal cell genes were absent (Fig. 2e). Conversely, *YAP-M* oncogene exhibited a strong suppressive effect on expression key signaling pathway genes, including ERK, PKA, and SHH cascades, in addition to genes characteristic of cortical progenitor populations such as Tri-IPCs, APCs, OPCs, and OBIN-IPCs (Fig. 2e). This is consistent with observations that human YAP-M-driven tumor cells lack classical glial progenitor markers [34,40]. YAP1

and WWTR1 are transcriptional co-activators. Reanalysis of ChIP-Seq and Cut&Run data for YAP1 and H3K27ac in both YAP-M-induced tumor cells and YAP1-expressing mouse neural stem cells identified multiple YAP-M target genes, characterized by distinct YAP-M binding sites, mainly in the promoter region [39]. These direct target genes included *Foxj1, Cryab, Anxa2, S100a11*, and *Ogn*, among others (Fig. 2f). Taken together, these loss- and gain-of-function analyses demonstrate that YAP signaling promotes cortical E-RG identity during cortical development and suppresses ERK, PKA, and SHH signaling (Fig. 2g).

SHH-SMO drives the establishment of cortical T-RG identity.

In all studied animals, a primary function of active SMO is to counteract the inhibitory effects of PKA on GLI transcription factors [26]. To investigate the *Smo* function in cortical RGs, we reanalyzed our previous scRNA-Seq data of cortical cells in *hGFAP-Cre; Smo*$^{F/F}$ mice E18.0 [15]. In the absence of *Smo*, cortical RG expression of *Gli1, Hhip*, *Ptch1, Egfr,* and *Olig2* was nearly undetectable (Fig. 3a-c). In contrast, signature genes associated with ERK signaling (*Hopx*, *Bmp7*, *Etv5, etc.*), PKA signaling (*Adcyap1r1, Adora2b, Gnas, Dio2*, and *Cxcl14*), YAP signaling (*Wwc2* and *Yap1*), and early ependymal cell markers (*Anxa2, Cryab, Foxj1*, and *S100a6*) exhibited significant upregulation (Fig. 3c). To further validate these findings, we conducted additional scRNA-Seq analysis of cortical cells isolated from *hGFAP-Cre; Smo*$^{F/F}$ mice and their *Smo*$^{F/F}$ littermate controls at P2. Notably, both E-RGs and T-RGs exhibited upregulation of ERK, PKA, and YAP signaling pathways (Extended Data Fig. 7a-c). Taken together, these findings indicate that SHH-SMO signaling promotes and maintains mouse cortical T-RG identity and facilitates their differentiation into Tri-IPCs by suppressing ERK, PKA, and YAP signaling (Fig. 3f).

PKA protects cortical N-RG identity

The reciprocal regulatory relationship between SHH signaling and PKA activity is well characterized: elevated PKA activity suppresses SHH signaling, while reduced PKA activity potentiates SHH pathway activation [26]. To further investigate the functional role of PKA in cortical RGs under conditions of *Smo* deficiency, we next performed a series of genetic analyses. At E15, we conducted IUE to ectopically express a dominant-negative form of PKA (*dnPKA-GFP*) in the cortices of both control (*Smo*$^{F/F}$) and *hGFAP-Cre; Smo*$^{F/F}$ mice. By E18, cells expressing dnPKA-GFP were isolated and analyzed by scRNA-Seq. Comparative analysis with FlashTag labeled cells from control (*Smo*$^{F/F}$) and *hGFAP-Cre; Smo*$^{F/F}$ E18 mice without dnPKA-IUE revealed the following findings in the cortical RGs of *hGFAP-Cre; Smo*$^{F/F}$ mice expressing dnPKA (Fig. 3a-c; Extended Data Fig. 8a, b): (1) complete ablation of PKA signaling; (2) significant upregulation of SHH pathway genes; (3) marked downregulation of ERK signaling; (4) suppression of YAP signaling; (5) blockade of early ependymal cell marker genes. Thus, the complete loss of PKA in cortical RGs directly leads to a

significant increase in SHH signaling, even without *Smo* function, which subsequently represses both ERK and YAP signaling. This result closely mirrors the phenotypes observed in our prior studies involving the overexpression of *Shh-N*, *Gli1*, *Gli2* activator, or *SmoM2* in cortical RGs [8,10,12,15]. Our results further solidify the role of PKA as the principal negative regulator of SHH signaling [26], in addition to its role as a suppressor of YAP signaling [28]. Immunostaining analysis of cortical sections 48-hours after *dnPKA* IUE revealed upregulated expression of EGFR, OLIG2, and GSX2 in the cortex of control and *hGFAP-Cre; Smo*$^{F/F}$ mice (Fig. 3d, e). This highlights the pivotal role of PKA signaling in N-RGs (neurogenic RGs) in protecting PyN genesis while simultaneously suppressing gliogenesis, including the production of ependymal cells, astrocytes, oligodendrocytes, and OBINs (Fig. 3g).

ERK safeguards both N-RG and T-RG identity

ERK signaling regulates multiple steps in cortical development [10,18,41]. To examine the function of ERK signaling, we used both *Emx1-Cre* and *hGFAP-Cre* lines to conditionally delete *Map2k1* and *Map2k2* (core downstream components of ERK; *Map2k1/2-dcko*) at progressively later stages [10,12]. scRNA-Seq analysis of E15.0 cortices revealed that SHH co-receptor *Gas1* expression was downregulated (Fig. 4a, b), and expression of ERK signaling downstream target genes was completely lost in N-RGs (Fig. 4b). This results in a significant decrease in the population of cortical N-RGs, concurrent with elevated *Eomes* expression (Fig. 4b). These cellular alterations were associated with pronounced microcephaly, as evidenced by a substantial reduction in overall brain size (Extended Data Fig. 9a-c), again demonstrating that ERK signaling in cortical N-RGs promotes self-renewal through enhanced cell proliferation while simultaneously inhibiting the generation of PyN-IPCs [12,42]. The upregulation of *Nr2f1* and *Fgfr3* expression in N-RGs confirmed that ERK signaling is essential for promoting the rostral cortical identity (Fig. 4b) [12,18]. Most importantly, we observed a subpopulation of cortical N-RGs exhibited *Adcyap1r1* expression, which was markedly downregulated in *Emx1-Cre; Map2k1/2* dcko mice (Fig. 4b). Conversely, there was upregulation of *Pde4d* expression in N-RGs (Fig. 4b). ERK-mediated phosphorylation of PDE4D3 at Ser579 inhibits PDE4 enzymatic activity, thereby potentiating cAMP-PKA signaling pathways [43]. Consequently, ERK deficiency initiates a signaling cascade characterized by attenuated PKA activity, leading to YAP signaling activation and elevated expression of early ependymal cell marker genes (Fig. 4b).

To further investigate the conserved functions of ERK signaling, we conducted a comprehensive reanalysis of our scRNA-Seq datasets from both *Emx1-Cre; Map2k1/2 dcko* and *hGFAP-Cre; Map2k1/2-dcko* mice at P2 [10]. While the *Emx1-Cre; Map2k1/2-dcko* mice displayed a substantial depletion of cortical RGs (Extended Data Fig. 10a-d), both mutants shared RGs defects, including: (1) loss of ERK signaling; (2) reduction of PKA signaling; (3) attenuation of SHH-SMO signaling; (4) failure to generate Tri-IPCs; (5) activation of YAP signaling; (6) upregulation of early

ependymal cell marker gene expression; and (7) increased production of ependymal cell populations (Extended Data Fig. 10a-d; Extended Data Fig. 11a-c). Our immunohistochemistry analyses yielded consistent results: a significant increase in YAP/TAZ nuclear localization within the cortical VZ at E16.0, followed by elevated numbers of CRYAB- and FOXJ1-expressing cells at P0 and P2 in *Emx1-Cre; Map2k1/2 dcko* mice compared to control littermates (Fig. 4c-e, Extended Data Fig. 10c, d).

To further investigate the function of ERK activation, we employed a gain-of-function approach using *Emx1-Cre; Mek1DD* mice, which specifically enhances ERK signaling in cortical RGs starting from E10.5. This resulted in a marked expansion of the cortical RG population while simultaneously inhibiting neuronal differentiation, ultimately leading to pronounced macrocephaly (Extended Data Fig. 9d-h).

In summary, during cortical neurogenesis, ERK and PKA signaling cooperate to suppress gliogenic YAP and SHH signaling pathways, thereby maintaining RG neurogenic potential (Fig. 4f). In *Emx1-Cre; Map2k1/2 dcko* mice, the degradation of pERK downregulates ERK and PKA signaling. While basal PKA activity potently inhibits SHH-SMO signaling, it is insufficient to counteract YAP activation, which occurs earlier than SHH-SMO signaling. This temporal signaling hierarchy directs cortical N-RGs to initially generate E-RGs, promoting ependymal cell formation while suppressing SHH signaling. Consequently, in the *Map2k1/2 dcko* there is a block of N-RGs to differentiate into T-RGs and their Tri-IPC progeny [10]. However, experimental enhancement of SHH signaling in cortical RGs of *Emx1-Cre; Map2k1/2 dcko* mice, which exhibit repressed YAP signaling, rescued Tri-IPC generation [10].

Discussion

During the early regional patterning stage of corticogenesis, the development is predominantly orchestrated by WNT, FGF, and BMP signaling [18,44,45]. This signaling network promotes RGs to generate PyNs through a precisely regulated inside-out developmental sequence [1-5]. Next, the neurogenic period of cortical RGs is regulated by a combination of intrinsic molecular mechanisms and extrinsic environmental cues. In mice, as YAP and SHH signaling pathways intensify in cortical RGs, they antagonize ERK and PKA signaling, reaching a critical threshold around E16.5. At this stage, a subpopulation of N-RGs in the medial cortex differentiates into E-RGs, which generate EP-IPCs [16]. Concurrently, N-RGs in the lateral cortex differentiate into T-RGs, initiating the production of Tri-IPCs [10,11,13].

During human corticogenesis, fRGs (full-span RGs) first undergo PyN genesis from GW8 to GW16 [4,13,14]. By GW16, following approximately 9 weeks of neurogenesis, the human fetal cortex has undergone significant expansion and harbors a substantial population of PyNs that require glial cell-derived support and nutrient supply from the developing vascular network. Concurrently, YAP and SHH signaling,

including CXCL12/CXCR signaling, progressively intensify in fRG cells. To accommodate the evolutionary pressure-driven expansion of PyN populations while concurrently meeting the heightened demand for glial cell production, human fRGs undergo a specialized division process, giving rise to oRGs and tRGs [4,13,14]. oRGs inherit the elongated basal processes from their fRGs and exhibit elevated levels of ERK and PKA activity, which are mutually reinforcing. ERK and PKA signaling enhancement suppresses gliogenic YAP and SHH signaling, thereby maintaining the neurogenic program in oRGs. In contrast, tRGs inherit the apical membrane domains from fRGs, maintaining direct contact with the lateral ventricle. Subsequently, the enhanced activation of the YAP and SHH signaling orchestrates the establishment of E-tRGs and T-tRGs identities, steering their differentiation into EP-IPCs and Tri-IPCs, respectively.

The loss of FGFR or ERK function in RGs results in remarkably similar cortical phenotypes [12,42]. FGFR-mediated ERK signaling plays an essential role in multiple aspects of cortical development, including neural induction, cortical regional patterning, RG cell proliferation, self-renewal, survival, growth, and promoting *BMP7* and *HOPX* expression [10,12,18,42]. In this study, we observed that ERK and PKA signaling establish a mutually reinforcing positive feedback loop, mediated through repressing gliogenic YAP and SHH signaling, which collectively drive the expansion of the cortical RG population and extend the neurogenic period. Both the ERK and PKA signaling pathways are tightly regulated by robust negative feedback mechanisms, which effectively prevent uncontrolled signal amplification and maintain cellular signaling homeostasis [24,25]. Interestingly, this regulatory program of FGF-ERK signaling exhibits remarkable evolutionary conservation, with homologous mechanisms identified in hemichordates and amphioxus, suggesting its origin dates back at least 500 million years [46]. Based on these findings, we propose that ERK signaling occupies a superior position in the regulatory hierarchy of signaling pathways governing cortical development and its surface-area expansion during evolution.

In summary, this study elucidates the molecular mechanisms responsible for the specification and lineage progression of distinct cortical RG subtypes across murine and human systems. It also uncovers fundamental principles that coordinate cortical neurogenesis, gliogenesis, expansion, which are conserved during evolution. Thereby these findings provide critical insights into the fundamental mechanisms of cortical development.

References

1 Kriegstein, A. & Alvarez-Buylla, A. The glial nature of embryonic and adult neural stem cells. *Annu Rev Neurosci* **32**, 149-184 (2009).

2 Florio, M. & Huttner, W. B. Neural progenitors, neurogenesis and the evolution of the neocortex. *Development* **141**, 2182-2194, doi:10.1242/dev.090571 (2014).

3 Lin, Y. *et al.* Behavior and lineage progression of neural progenitors in the mammalian cortex. *Curr Opin Neurobiol* **66**, 144-157, doi:10.1016/j.conb.2020.10.017 (2021).

4 Yang, Z. The Principle of Cortical Development and Evolution. *Neurosci Bull* **41**, 461-485, doi:10.1007/s12264-024-01259-2 (2025).

5 Rakic, P. A century of progress in corticoneurogenesis: from silver impregnation to genetic engineering. *Cereb Cortex* **16 Suppl 1**, i3-17, doi:10.1093/cercor/bhk036 (2006).

6 Molnar, Z. *et al.* New insights into the development of the human cerebral cortex. *J Anat* **235**, 432-451, doi:10.1111/joa.13055 (2019).

7 Ortiz-Alvarez, G. & Spassky, N. One progenitor to generate them all: new evidence for multi-fated neural progenitors. *Curr Opin Neurobiol* **66**, 186-194, doi:10.1016/j.conb.2020.10.013 (2021).

8 Zhang, Y. *et al.* Cortical Neural Stem Cell Lineage Progression Is Regulated by Extrinsic Signaling Molecule Sonic Hedgehog. *Cell Rep* **30**, 4490-4504 e4494, doi:10.1016/j.celrep.2020.03.027 (2020).

9 Wang, L. *et al.* Molecular and cellular dynamics of the developing human neocortex. *Nature*, doi:10.1038/s41586-024-08351-7 (2025).

10 Gao, Y. *et al.* NOTCH, ERK, and SHH signaling respectively control the fate determination of cortical glia and olfactory bulb interneurons. *Proc Natl Acad Sci U S A* **122**, e2416757122, doi:10.1073/pnas.2416757122 (2025).

11 Li, X. *et al.* Decoding Cortical Glial Cell Development. *Neurosci Bull* **37**, 440-460, doi:10.1007/s12264-021-00640-9 (2021).

12 Sun, M. *et al.* ERK signaling expands mammalian cortical radial glial cells and extends the neurogenic period. *Proc Natl Acad Sci U S A* **121**, e2314802121, doi:10.1073/pnas.2314802121 (2024).

13 Yang, L., Li, Z., Liu, G., Li, X. & Yang, Z. Developmental Origins of Human Cortical Oligodendrocytes and Astrocytes. *Neurosci Bull* **38**, 47-68, doi:10.1007/s12264-021-00759-9 (2022).

14 Nowakowski, T. J., Pollen, A. A., Sandoval-Espinosa, C. & Kriegstein, A. R. Transformation of the Radial Glia Scaffold Demarcates Two Stages of Human Cerebral Cortex Development. *Neuron* **91**, 1219-1227, doi:10.1016/j.neuron.2016.09.005 (2016).

15 Li, Z. *et al.* BMP7 expression in mammalian cortical radial glial cells increases the length of the neurogenic period. *Protein Cell* **15**, 21-35, doi:10.1093/procel/pwad036 (2024).

16 Kyrousi, C., Lygerou, Z. & Taraviras, S. How a radial glial cell decides to become a multiciliated ependymal cell. *Glia* **65**, 1032-1042, doi:10.1002/glia.23118 (2017).

17 Trevino, A. E. *et al.* Chromatin and gene-regulatory dynamics of the developing human cerebral cortex at single-cell resolution. *Cell* **184**, 5053-5069 e5023, doi:10.1016/j.cell.2021.07.039 (2021).

18 Hoch, R. V., Rubenstein, J. L. & Pleasure, S. Genes and signaling events that establish regional patterning of the mammalian forebrain. *Semin Cell Dev Biol* **20**, 378-386, doi:10.1016/j.semcdb.2009.02.005 (2009).
19 Vaudry, D. *et al.* Pituitary adenylate cyclase-activating polypeptide and its receptors: 20 years after the discovery. *Pharmacol Rev* **61**, 283-357, doi:10.1124/pr.109.001370 (2009).
20 Fredholm, B. B. *et al.* Structure and function of adenosine receptors and their genes. *Naunyn Schmiedebergs Arch Pharmacol* **362**, 364-374, doi:10.1007/s002100000313 (2000).
21 Cereijo, R. *et al.* CXCL14, a Brown Adipokine that Mediates Brown-Fat-to-Macrophage Communication in Thermogenic Adaptation. *Cell Metab* **28**, 750-763 e756, doi:10.1016/j.cmet.2018.07.015 (2018).
22 Kohrle, J. & Fradrich, C. Deiodinases control local cellular and systemic thyroid hormone availability. *Free Radic Biol Med* **193**, 59-79, doi:10.1016/j.freeradbiomed.2022.09.024 (2022).
23 Feige, J. J. & Baird, A. Basic fibroblast growth factor is a substrate for protein phosphorylation and is phosphorylated by capillary endothelial cells in culture. *Proc Natl Acad Sci U S A* **86**, 3174-3178, doi:10.1073/pnas.86.9.3174 (1989).
24 Stork, P. J. & Schmitt, J. M. Crosstalk between cAMP and MAP kinase signaling in the regulation of cell proliferation. *Trends Cell Biol* **12**, 258-266, doi:10.1016/s0962-8924(02)02294-8 (2002).
25 Houslay, M. D. & Kolch, W. Cell-type specific integration of cross-talk between extracellular signal-regulated kinase and cAMP signaling. *Mol Pharmacol* **58**, 659-668 (2000).
26 Kong, J. H., Siebold, C. & Rohatgi, R. Biochemical mechanisms of vertebrate hedgehog signaling. *Development* **146**, doi:10.1242/dev.166892 (2019).
27 Rao, R., Salloum, R., Xin, M. & Lu, Q. R. The G protein Galphas acts as a tumor suppressor in sonic hedgehog signaling-driven tumorigenesis. *Cell Cycle* **15**, 1325-1330, doi:10.1080/15384101.2016.1164371 (2016).
28 Zhong, Z., Jiao, Z. & Yu, F. X. The Hippo signaling pathway in development and regeneration. *Cell Rep* **43**, 113926, doi:10.1016/j.celrep.2024.113926 (2024).
29 Lavado, A. *et al.* YAP/TAZ maintain the proliferative capacity and structural organization of radial glial cells during brain development. *Developmental biology* **480**, 39-49, doi:10.1016/j.ydbio.2021.08.010 (2021).
30 Park, R. *et al.* Yap is required for ependymal integrity and is suppressed in LPA-induced hydrocephalus. *Nat Commun* **7**, 10329, doi:10.1038/ncomms10329 (2016).
31 White, S. M. *et al.* YAP/TAZ Inhibition Induces Metabolic and Signaling Rewiring Resulting in Targetable Vulnerabilities in NF2-Deficient Tumor Cells. *Dev Cell* **49**, 425-443 e429, doi:10.1016/j.devcel.2019.04.014 (2019).
32 Deng, Y. *et al.* A reciprocal regulatory loop between TAZ/YAP and G-protein Galphas regulates Schwann cell proliferation and myelination. *Nat Commun* **8**, 15161, doi:10.1038/ncomms15161 (2017).
33 Kim, J. *et al.* Actin remodelling factors control ciliogenesis by regulating YAP/TAZ activity and vesicle trafficking. *Nat Commun* **6**, 6781, doi:10.1038/ncomms7781 (2015).

34 Hu, X. *et al.* Nuclear condensates of YAP fusion proteins alter transcription to drive ependymoma tumourigenesis. *Nat Cell Biol* **25**, 323-336, doi:10.1038/s41556-022-01069-6 (2023).
35 Krishnan, V. *et al.* Mediation of Sonic hedgehog-induced expression of COUP-TFII by a protein phosphatase. *Science* **278**, 1947-1950, doi:10.1126/science.278.5345.1947 (1997).
36 Forget, A. *et al.* Shh signaling protects Atoh1 from degradation mediated by the E3 ubiquitin ligase Huwe1 in neural precursors. *Dev Cell* **29**, 649-661, doi:10.1016/j.devcel.2014.05.014 (2014).
37 Cotton, J. L. *et al.* YAP/TAZ and Hedgehog Coordinate Growth and Patterning in Gastrointestinal Mesenchyme. *Dev Cell* **43**, 35-47 e34, doi:10.1016/j.devcel.2017.08.019 (2017).
38 Qi, S. *et al.* WWC proteins mediate LATS1/2 activation by Hippo kinases and imply a tumor suppression strategy. *Mol Cell* **82**, 1850-1864 e1857, doi:10.1016/j.molcel.2022.03.027 (2022).
39 Hu, X., Eastman, A. E. & Guo, S. Cell cycle dynamics in the reprogramming of cellular identity. *FEBS Lett* **593**, 2840-2852, doi:10.1002/1873-3468.13625 (2019).
40 Pajtler, K. W. *et al.* YAP1 subgroup supratentorial ependymoma requires TEAD and nuclear factor I-mediated transcriptional programmes for tumorigenesis. *Nat Commun* **10**, 3914, doi:10.1038/s41467-019-11884-5 (2019).
41 Lavoie, H., Gagnon, J. & Therrien, M. ERK signalling: a master regulator of cell behaviour, life and fate. *Nat Rev Mol Cell Biol* **21**, 607-632, doi:10.1038/s41580-020-0255-7 (2020).
42 Kang, W., Wong, L. C., Shi, S. H. & Hebert, J. M. The transition from radial glial to intermediate progenitor cell is inhibited by FGF signaling during corticogenesis. *J Neurosci* **29**, 14571-14580, doi:10.1523/JNEUROSCI.3844-09.2009 (2009).
43 Hoffmann, R., Baillie, G. S., MacKenzie, S. J., Yarwood, S. J. & Houslay, M. D. The MAP kinase ERK2 inhibits the cyclic AMP-specific phosphodiesterase HSPDE4D3 by phosphorylating it at Ser579. *Embo J* **18**, 893-903, doi:10.1093/emboj/18.4.893 (1999).
44 Backman, M. *et al.* Effects of canonical Wnt signaling on dorso-ventral specification of the mouse telencephalon. *Developmental biology* **279**, 155-168, doi:10.1016/j.ydbio.2004.12.010 (2005).
45 Gunhaga, L. *et al.* Specification of dorsal telencephalic character by sequential Wnt and FGF signaling. *Nat Neurosci* **6**, 701-707, doi:10.1038/nn1068 (2003).
46 Pani, A. M. *et al.* Ancient deuterostome origins of vertebrate brain signalling centres. *Nature* **483**, 289-294, doi:10.1038/nature10838 (2012).
47 Gorski, J. A. *et al.* Cortical excitatory neurons and glia, but not GABAergic neurons, are produced in the Emx1-expressing lineage. *J Neurosci* **22**, 6309-6314 (2002).
48 Zhuo, L. *et al.* hGFAP-cre transgenic mice for manipulation of glial and neuronal function in vivo. *Genesis* **31**, 85-94 (2001).
49 Srinivasan, L. *et al.* PI3 kinase signals BCR-dependent mature B cell survival. *Cell* **139**, 573-586, doi:10.1016/j.cell.2009.08.041 (2009).
50 Long, F., Zhang, X. M., Karp, S., Yang, Y. & McMahon, A. P. Genetic manipulation of hedgehog signaling in the endochondral skeleton reveals a direct role in the regulation

of chondrocyte proliferation. *Development* **128**, 5099-5108, doi:10.1242/dev.128.24.5099 (2001).

51 Clegg, C. H., Correll, L. A., Cadd, G. G. & McKnight, G. S. Inhibition of intracellular cAMP-dependent protein kinase using mutant genes of the regulatory type I subunit. *J Biol Chem* **262**, 13111-13119 (1987).

52 Telley, L. *et al.* Sequential transcriptional waves direct the differentiation of newborn neurons in the mouse neocortex. *Science* **351**, 1443-1446, doi:10.1126/science.aad8361 (2016).

53 Govindan, S., Oberst, P. & Jabaudon, D. In vivo pulse labeling of isochronic cohorts of cells in the central nervous system using FlashTag. *Nat Protoc* **13**, 2297-2311, doi:10.1038/s41596-018-0038-1 (2018).

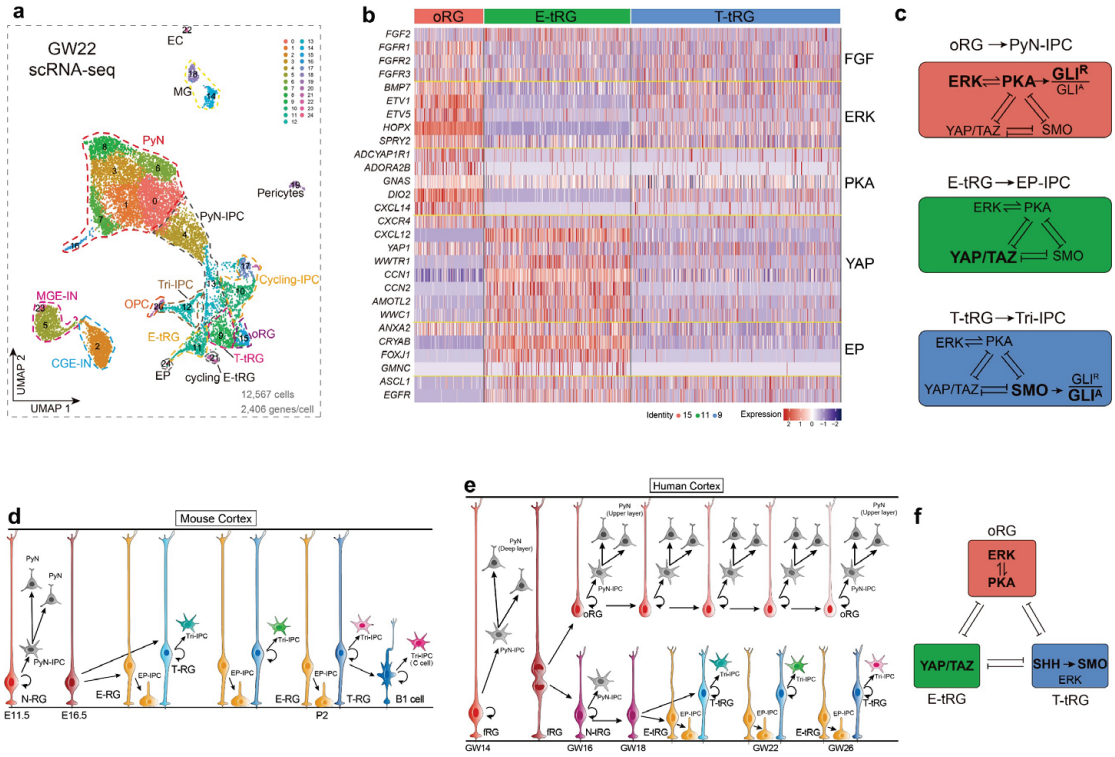

Fig. 1 | The molecular signatures of human cortical oRGs, E-tRGs, and T-tRGs. **a**, Reanalysis of scRNA-Seq data derived from human cortical tissue at GW22 [17]. UMAP visualization with cells colored by cluster. **b**, Heatmap illustrating differentially expressed genes among human cortical oRGs, E-tRGs, and T-tRGs. EP, ependymal cells. **c**, oRGs exhibited elevated ERK and PKA signaling, while E-tRGs exhibited enhanced YAP signaling. A subset of T-tRGs expressed genes (such as *EGFR* and *ASCL1,* in **b**) in response to elevated SHH-SMO signaling. ERK/PKA, YAP, and SHH signaling reciprocally inhibit each other in human cortical RGs. **d, e**. Mouse and human cortical RG cell lineage progression. **f**. oRGs, E-tRGs, and T-tRGs maintain their distinct identities through mutual repression mechanisms.

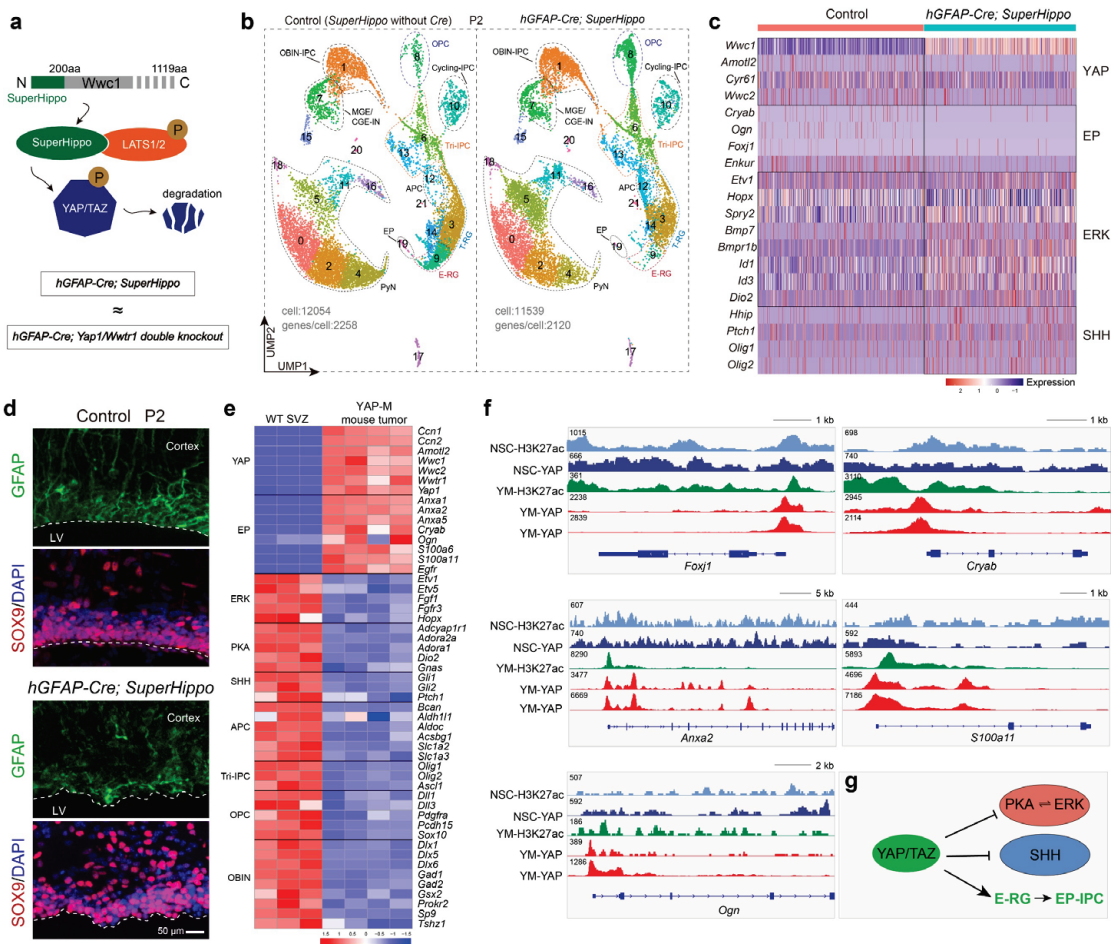

Fig. 2 | YAP signaling promotes the cortical E-RG identity. a, A *SuperHippo* minigene has been engineered to robustly inhibit YAP signaling (YAP/TAZ activity). **b**, Annotation of cortical cell clusters in P2 control (*SuperHippo* heterozygotes without *hGFAP-Cre*) and *hGFAP-Cre; SuperHippo* mice. **c**, Heatmap illustrating differentially expressed genes in cortical T-RGs (cluster 3 in **b**). **d**. Immunostaining reveals disruption of the cortical ventricular surface and the loss of apical SOX9- and GFAP-expressing immature ependymal cells in the P2 *hGFAP-Cre; SuperHippo* cortex. LV, lateral ventricle. **e**. Bulk RNA-Seq analysis. Heatmap of differentially expressed genes between the SVZ cells of wild-type control mice (n=3) and the tumor cells derived from ~P20 mice transfected with YAP-M at E14.5 (n=4 independent replicates) [34]. **f**. ChIP-Seq analysis showing YAP1 binding and H3K27ac modification profiles on early ependymal cell marker gene loci in YAP-M tissue and YAP-expressing wild type neural stem cells. This analysis is based on reanalyzed data from a previous study [34]. **g**. YAP signaling establishes and maintains the molecular identity of cortical E-RGs and drives their differentiation into ependymal cell lineages through reciprocal repression with the PKA, ERK, and SHH signaling pathways.

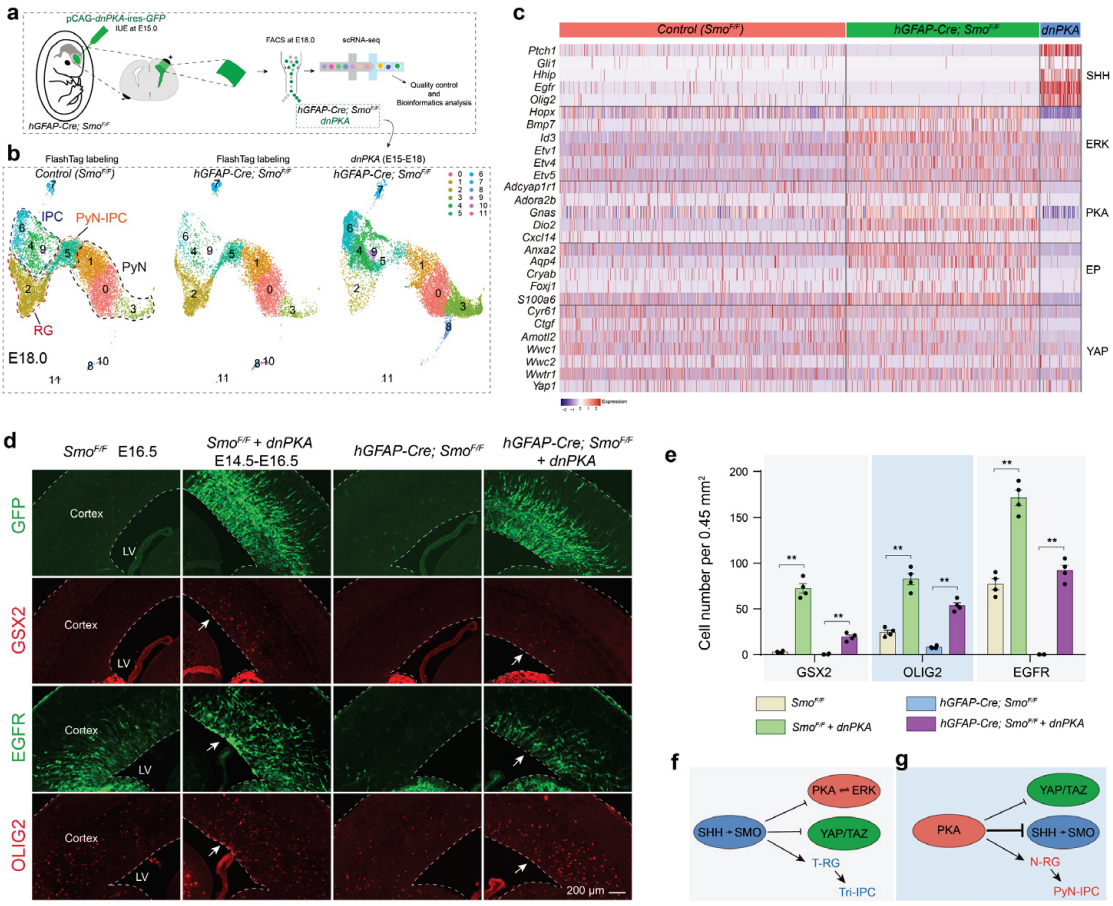

Fig. 3 | The functional interplay between SHH and PKA signaling in the cortical RGs. a, Scheme for overexpressing *pCAG-dnPKA-GFP* plasmids into the cortical VZ of *Smo*$^{F/F}$ control and *hGFAP-Cre; Smo*$^{F/F}$ mouse embryos at E15 by IUE, and scRNA-Seq of GFP-expressing cells at E18.0. **b**, Annotation of cortical cell clusters. **c**, Heatmap illustrating gene expression cortical RGs of *Smo*$^{F/F}$, *hGFAP-Cre; Smo*$^{F/F}$, and *hGFAP-Cre; Smo*$^{F/F}$ mice with IUE of *dnPKA*. **d, e,** Immunostaining reveals a marked expansion of GSX2-, EGFR-, and OLIG2-positive progenitors in the cortical VZ/SVZ following IUE of *dnPKA* (PKA signaling completely ablation). **f,** SHH-SMO signaling promotes the identity of T-RGs. **g**, PKA signaling maintains cortical N-RG identity by strongly inhibiting SHH signaling and moderately suppressing YAP signaling.

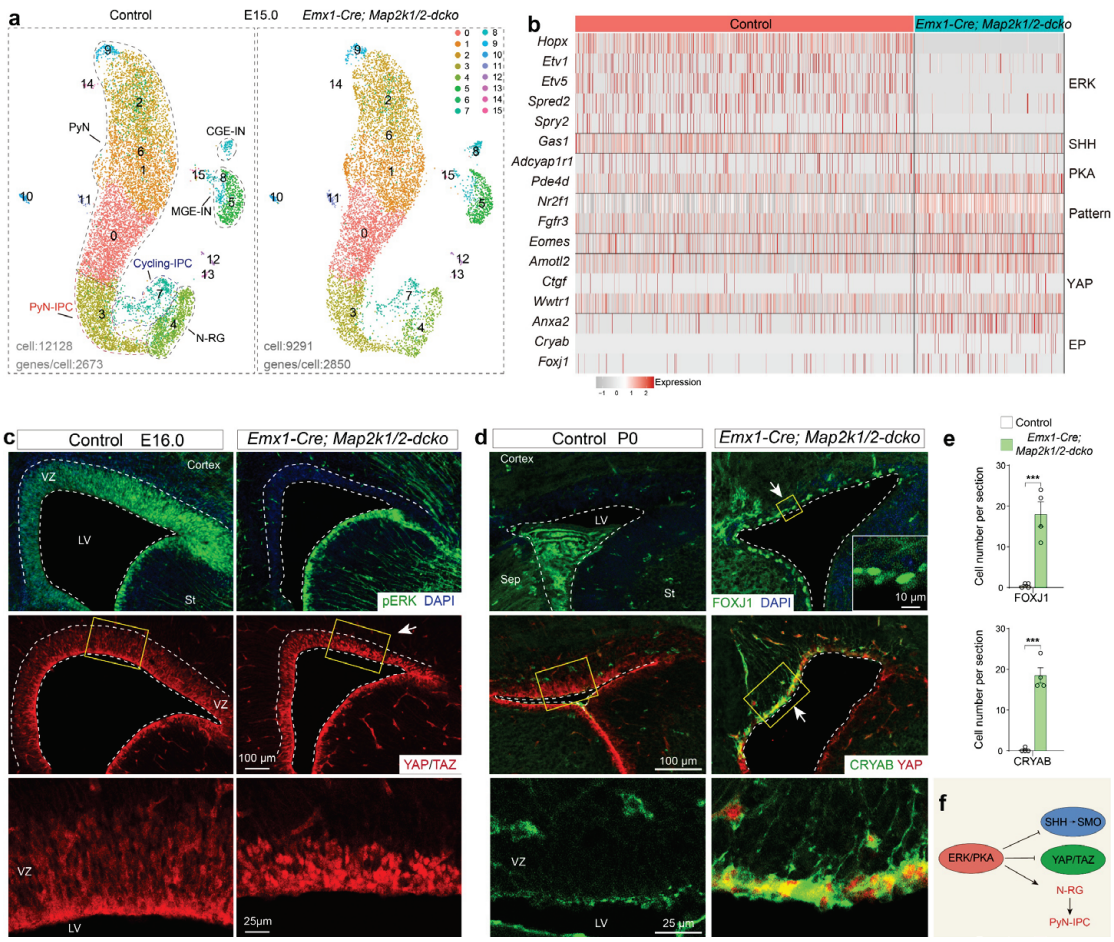

Fig. 4 | ERK signaling enhances PKA signaling and suppresses YAP signaling. **a**, UMAP showing annotated cell clusters based on scRNA-Seq of E15.0 control and *Emx1-cre; Map2k1/2 dcko* cortical cells. N-RG: PyN neurogenic radial glia. **b**, Heatmap showing the expression of selected ERK, SHH, PKA, and YAP signaling response genes, as well as cortical regional and early cortical ependymal cell genes, in cortical N-RGs of *Emx1-Cre; Map2k1/2-dcko* mice compared to littermate controls at E15.0. **c**, pERK (phosphorylated ERK) staining is lost, and nuclear localization of YAP/TAZ proteins is increased specifically in cortical RGs of *Emx1-Cre; Map2k1/2-dcko* mice at E16.0. **d, e**, FOXJ1- and CRYAB-expressing cells are observed in the VZ of *Emx1-Cre; Map2k1/2-dcko* mice, whereas their expression is undetectable in controls at P0. Sep, septum; St, striatum. **f**, ERK/PKA signaling maintains the neurogenic program of cortical N-RGs by repressing gliogenic YAP and SHH signaling pathways.

Methods

Animals

All procedures involving animals were approved by and performed in accordance with the guidelines of the Fudan University Shanghai Medical College Animal Ethics Committee. *Emx1-Cre* (JAX no. 005628) [47], *hGFAP-Cre* (JAX no. 004600) [48], *Rosa*^{Mek1DD} (JAX no. 012352) [49], *Smo flox* (JAX no.004526) [50], *Map2k1* (exon 2) floxed and *Map2k2* (exon 4-9) floxed mice [12] were described previously. *SuperHippo* mice were provided by Professor Faxing Yu at Fudan University [38]. The day of detecting a vaginal plug was designated as E0.5. The day of birth was designated as P0. The sexes of the embryonic and early postnatal mice were not determined. For immunostaining analysis, normally, brains from 3-5 independent experiments were processed (n values refer to numbers of brains analyzed).

Tissue preparation

Embryos were isolated from deeply anesthetized pregnant mice. Brains were dissected and fixed overnight in 4% paraformaldehyde (PFA) pre-treated with diethylpyrocarbonate (DEPC). Postnatal mice were deeply anesthetized and transcardially perfused with phosphate-buffered saline (PBS), followed by 4% PFA. All brains were post-fixed overnight in 4% PFA at 4°C and subsequently dehydrated in 30% sucrose for at least 24 hours. The brains were then embedded in O.C.T. compound (Sakura Finetek) and stored at -80°C. For analysis, mouse brains were sectioned into 20-μm-thick slices.

Plasmid construction

pCAG-ires-GFP plasmid was from Addgene (Addgene #11150). The mouse *dnPKA* cDNA represents a dominant-negative form of PKA [51]. This variant is derived from PKA-RIa, which is encoded by the *Prkar1a* gene, and is characterized by mutations at the cAMP binding sites, rendering it unresponsive to cAMP. The *dnPKA* cDNA was subsequently cloned into the *pCAG-GFP* vector to generate *pCAG-dnPKA-ires-GFP* plasmids.

In Utero Electroporation (IUE)

In utero electroporation was performed as described previously [8]. Briefly, pregnant mice were anesthetized using an animal anesthesia machine with isoflurane. A plasmid solution (final concentration: 1–2 μg/μl for each plasmid, 0.5 μl per embryo), mixed with 0.05% Fast Green (Sigma), was injected into the lateral ventricle of embryos using a beveled glass micropipette. Five electrical pulses (duration: 50 ms) were delivered at optimized voltages across the uterine wall, with a 950-ms interval

between pulses, using a pair of 7-mm platinum electrodes (BTX, Tweezertrode 45-0488, Harvard Apparatus) connected to an electroporator (BTX, ECM830). The applied voltages were adjusted according to embryonic age: 33 V for E14, 35 V for E15, and 38 V for E18. Electroporated brains were analyzed at specified time points, as indicated in the main text.

FlashTag labeling

FlashTag labeling was performed via in utero injection, and the FlashTag-labeled live cells were subsequently isolated using fluorescence-activated cell sorting (FACS) [52,53]. To label embryonic day 15.5 (E15.5) cortical progenitors, CellTrace Yellow solution (Life Technologies, #C34567; 0.5 µl of 10 mM) was injected into the lateral ventricles of *SuperHippo* with or without *hGFAP-Cre* and *Emx1-Cre*, mice at E15.50, with analysis performed at E16.5. To label E17.0 progenitors, CellTrace Yellow solution was injected into the mouse lateral ventricles of $Smo^{F/F}$ and *hGFAP-Cre;* $Smo^{F/F}$ mice at embryonic day 17.0 (E17.0), with analysis performed at E18. To label P0 progenitors, the CellTrace solution was injected into the lateral ventricles of the following groups at postnatal day 0 (P0), with analysis conducted at P2: Control (*SuperHippo* without *Cre*), *hGFAP-Cre; SuperHippo*, $Smo^{F/F}$, *hGFAP-Cre;* $Smo^{F/F}$, *hGFAP-Cre; Map2k1/2-dcko*, and *Emx1-Cre; Map2k1/2-dcko* mice. Mice were sacrificed, and brains were immediately removed and submerged in fresh ice-cold Hanks' balanced salt solution (HBSS; Gibco, 14175-095). Cortices were dissected, dissociated into single-cell suspensions, and subjected to FACS to purify FlashTag-labeled cells. Single-cell RNA sequencing (scRNA-Seq) was performed on FACS-sorted cells using the 10X Genomics platform.

Immunohistochemistry

Immunohistochemistry was performed on 20-µm coronal sections of mouse brains using standard protocols. Sections were rinsed with Tris-buffered saline (TBS; 0.01 M Tris–HCl, 0.9% NaCl, pH 7.4) for 10 minutes, permeabilized with 0.5% Triton-X-100 in TBS for 30 minutes at room temperature (RT), and blocked in a solution of 5% donkey serum and 0.5% Triton-X-100 in TBS (pH 7.2) for 2 hours. After blocking, sections were incubated with primary antibodies diluted in blocking buffer overnight at 4°C. The following day, sections were washed three times with TBS (10 minutes each) and incubated with secondary antibodies (1:500; Jackson ImmunoResearch) for 2 hours in the dark at RT. After three additional TBS washes (10 minutes each), sections were counterstained with 4',6-diamidino-2-phenylindole (DAPI; Sigma, 200 ng/mL) for 2 minutes.

The following primary antibodies were used in this study (Table 1):

primary Ab	Species	Dilution	Manufacturer	Cat. No.
CUX1	Rabbit	1:200	Santa Cruz	sc-13024
CRYAB	Mouse	1:500	Abcam	ab13496
EGFR	Goat	1:1000	R&D System	BAF1280
EOMES	Guinea pig	1:500	Oasis Biofarm	OB-PGP022
FOXJ1	Mouse	1:1000	Invitrogen	14-9965-80
GFP	Chicken	1:3000	Aves labs	GFP-1020
GFAP	Rabbit	1:1000	Dako	Z0334
GSX2	Rabbit	1:500	Millipore	ABN162
NEUN	Rabbit	1:1000	Biosensis	R-3770-100
OLIG2	Rabbit	1:500	Millipore	AB9610
OLIG2	Rat	1:500	Oasis Biofarm	OB-PRB009
pERK1/2	Rabbit	1:400	Cell Signaling	#4370
SOX9	Rabbit	1:1000	Abcam	ab185966
YAP/TAZ	Rabbit	1:1500	Cell Signaling	14074S

scRNA-Seq

This study produced a comprehensive collection of 11 novel scRNA-Seq datasets (Table 2).

Number	Age	Genotype	Notes
1	E15.0	*Map2k1/2* (without *Cre*)	Whole cortex
2	E15.0	*Emx1-Cre; Map2k1/2-dcko*	Whole cortex
3	E16.5	*Wild-type littermate*	FlashTag labeling at E15.5
4	E16.5	*hGFAP-Cre; SuperHippo*	FlashTag labeling at E15.5
5	E16.5	*SuperHippo* (without *Cre*)	FlashTag labeling at E15.5
6	E16.5	*Emx1-Cre; SuperHippo*	FlashTag labeling at E15.5
7	E18.0	*hGFAP-Cre;* $Smo^{F/F}$ + *dnPKA*	IUE (*dnPKA*) labeling at E15.0
8	P2	*SuperHippo* (without *Cre*)	FlashTag labeling at P0
9	P2	*hGFAP-Cre; SuperHippo*	FlashTag labeling at P0
10	P2	$Smo^{F/F}$	FlashTag labeling at P0
11	P2	*hGFAP-Cre;* $Smo^{F/F}$	FlashTag labeling at P0

Briefly, mouse cortices were dissociated into single-cell suspensions, and selected samples were screened by FACS prior to single-cell sequencing. scRNA-Seq libraries were generated using the Chromium droplet-based platform (10X Genomics) according to the manufacturer's instructions (manual document part number: CG00052 Rev C). Purified cDNA libraries were quantified using an Agilent 2100 Bioanalyzer and sequenced on an Illumina NovaSeq 6000 platform.

scRNA-Seq data analysis

scRNA-Seq reads were aligned to the mm10 reference genome and quantified using 'cellranger count' (10x Genomics, v.7.1.0). Count data was further processed using the 'Seurat' R package (v.5.1.0). Genes detected in fewer than three cells, cells with fewer than 500 detected genes, and cells with more than 10% mitochondrial gene content were filtered out. After filtering, the number of cells in each dataset was as follows:

E15.0 cortex: *Map2k1/2* (without *Cre*) 12,128 cells, 2,673 genes/cell, *Emx1-Cre; Map2k1/2-dcko* mice, 9,291 cells, 2,850 genes/cell; E16.5 FACS cortical progenitors: wild-type 14,800 cells, 1,504 genes/cell, *hGFAP-Cre; SuperHippo* 13,171 cells, 1,544 genes/cell; E16.5 FACS cortical progenitors: *SuperHippo* without *Emx1-Cre* 13,194 cells, 2,582 genes/cell, *Emx1-Cre; SuperHippo* mice, 14,641 cells, 2,616 genes/cell; E18.0 FACS cortical progenitors labeled by dnPKA-GFP in *hGFAP-Cre;* $Smo^{F/F}$ 11,508 cells, 2,369 genes/cell; P2 FACS cortical progenitors: control ($Smo^{F/F}$), 14,292 cells, 2,498 genes/cell; *hGFAP-Cre;* $Smo^{F/F}$ mice, 7,694 cells, 2,681 genes/cell; control (*SuperHippo* heterozygotes without *hGFAP-Cre*), 12,054 cells, 2,258 genes/cell; *hGFAP-Cre; SuperHippo* mice, 11,539 cells, 2,120 genes/cell. These 11 novel scRNA-Seq data have been deposited in the GEO under the accession number GSE293205.

Gene expression data were normalized using the global-scaling method "LogNormalize". The top 2,000 highly variable genes were identified with the FindVariableFeatures function using the vst method. To minimize the influence of the cell cycle on clustering and dimensionality reduction, cell cycle-associated gene sets were used to score the cell phase of each cell with the CellCycleScoring function, and the difference between G2M and S phase scores was regressed out using the ScaleData function. The scaled z-scored residuals were used for Principal Component Analysis (PCA). Statistically significant principal components, identified through a resampling test, were retained for FindNeighbors and FindClusters analysis. Uniform Manifold Approximation and Projection (UMAP) was used for visualization of cell clustering. Differentially expressed genes (DEGs) among clusters were identified using the Wilcoxon rank sum test, comparing cells in each cluster against all other cells.

Image acquisition and analysis

All brain section images in this study were acquired using an Olympus VS120 Automated Slide Scanner (10X, 20X) and an FV3000 confocal microscope system (40X). Images were processed using Adobe Photoshop for clarity, false colorization, and overlay as needed. Both Adobe Photoshop and Adobe Illustrator were used to adjust images without altering the original data.

Quantification and statistical analysis

Quantitative images were acquired using the Olympus VS120 Automated Slide Scanner (10X or 20X). Statistical analyses were performed using GraphPad Prism 10 and IBM SPSS Statistics 29.0. For each experiment, at least three control or mutant mouse samples were analyzed. The following quantifications were performed:

1. Quantification of GSX2-, OLIG2-, and EGFR-positive cells in the cortical VZ/SVZ (width: 1200 pixels; height: 800 pixels) at E18 in *Smo*$^{F/F}$, *Smo*$^{F/F}$*+dnPKA*, *hGFAP-Cre; Smo*$^{F/F}$, and *hGFAP-Cre; Smo*$^{F/F}$*+dnPKA* mouse brains (see Fig. 3).

2. Quantification of FOXJ1- and CRYAB-positive cells in the cortex of control and *Emx1-Cre; Map2k1/2-dcko* mice at P0. FOXJ1- and CRYAB-positive cells in the dorsal cortical VZ/SVZ were counted. Four brain slices from corresponding locations were analyzed per sample (see Fig. 4).

3. Quantification of GSX2^{+} and OLIG2^{+} cells in the cortex of control and *hGFAP-Cre; SuperHippo* mice. Four brain slices from corresponding positions were selected per sample, and GSX2^{+} and OLIG2^{+} cells in the entire VZ/SVZ region were counted (see Extended Data Fig. 4 and Extended Data Fig. 5).

4. Quantification of cortical area at P21 in control and *Emx1-Cre; Map2k1/2-dcko* mice. Six brain slices from corresponding positions were analyzed per sample, and the cortical area was measured using Photoshop (see Extended Data Fig. 9c).

5. Quantification of EOMES+ cells in the cortical VZ (width: 300 pixels; height: 300 pixels) of control and *Emx1-Cre; Rosa*^{Mek1DD} mice at E13.5. Four brain slices from corresponding positions were analyzed per sample (see Extended Data Fig. 9e).

6. Quantification of cortical area at P76 in control and *Emx1-Cre; Rosa*^{Mek1DD} mice. Six brain slices from corresponding positions were analyzed per sample, and the cortical area was measured using Photoshop (see Extended Data Fig. 9h).

7. Quantification of FOXJ1- and CRYAB-positive cells in the cortex of control and *Emx1-Cre; Map2k1/2-dcko* mice at P2. FOXJ1- and CRYAB-positive cells in the dorsal cortical VZ/SVZ were counted. Four brain slices from corresponding locations were analyzed per sample (see Extended Data Fig. 10d). Data are presented as mean ± SEM. Statistical significance for single comparisons was determined using unpaired t-tests. A P-value < 0.05 was considered statistically significant (*P < 0.05, **P < 0.01, ***P < 0.001).

Data availability

The datasets (scRNA-Seq from 11 samples, Table 2) generated during the current study are available in the Gene Expression Omnibus (GEO: GSE293205). The E18.0 *Smo*$^{F/F}$ (control) and *hGFAP-Cre; Smo*$^{F/F}$ mouse cortex scRNA-Seq data were used from our previous study [15] (GSE221389). The P2 *Emx1-Cre; Map2k1/2-dcko* and P2 *hGFAP-Cre; Map2k1/2-dcko* mouse cortex scRNA-Seq data were used from our previous studies (GSE274547). Bulk RNA-Seq data from the SVZ of wild-type control mice (n=3) and tumor cells derived from ~P20 mice transfected with YAP-M at E14.5 (n=4), and ChIP-Seq and Cut&Run data for YAP1 and H3K27ac in both YAP-M-induced tumor cells and YAP1-expressing mouse neural stem cells were used in previous studies [34] (GSE181867).

Code availability

The data analysis in this study was performed using R, primarily based on the Seurat (v5.1.0) and ggplot2 (v3.5.1) packages. All analysis steps, including integration, clustering, dimensionality reduction, differential expression analysis, and visualization, were conducted using standard functions from these packages. No new computational methods or custom scripts were developed in this study.

Acknowledgments

We sincerely thank Professor John L. Rubenstein for his insightful comments and critical editing of the manuscript. We are also grateful to Professors Arnold Kriegstein and Bin Chen for their valuable feedback and constructive critiques on our data. We thank Professor Faxing Yu for sharing the *SuperHippo* mice. This study was supported by the Ministry of Science and Technology of China (STI2030-2021ZD0202300), National Natural Science Foundation of China (NSFC 31820103006, 32070971, 32100768, 32200776, and 32200792), China Postdoctoral Science Foundation (2024T170179), Shanghai Municipal Science and Technology Major Project (No.2018SHZDZX01), ZJ Lab, and Shanghai Center for Brain Science and Brain-Inspired Technology.

Author contributions

Conceptualization: Z.Y. Data curation: T.F., Z.Z., Z.X. and J.L. Funding acquisition: Z.Z., Z.X., T.M., and Z.Y. Investigation: Z.Z., Z.X., T.F., J.L., F.Y., C.Y., W.Z., Z.S., Y.G., M.S., Z.L., J.D., and X.L. Resources: Z.Y. Supervision: Z.Y. Writing: Z.Y. All of the authors contributed to reviewing and editing of the manuscript.

Competing Interest Statement: The authors declare no competing interest.

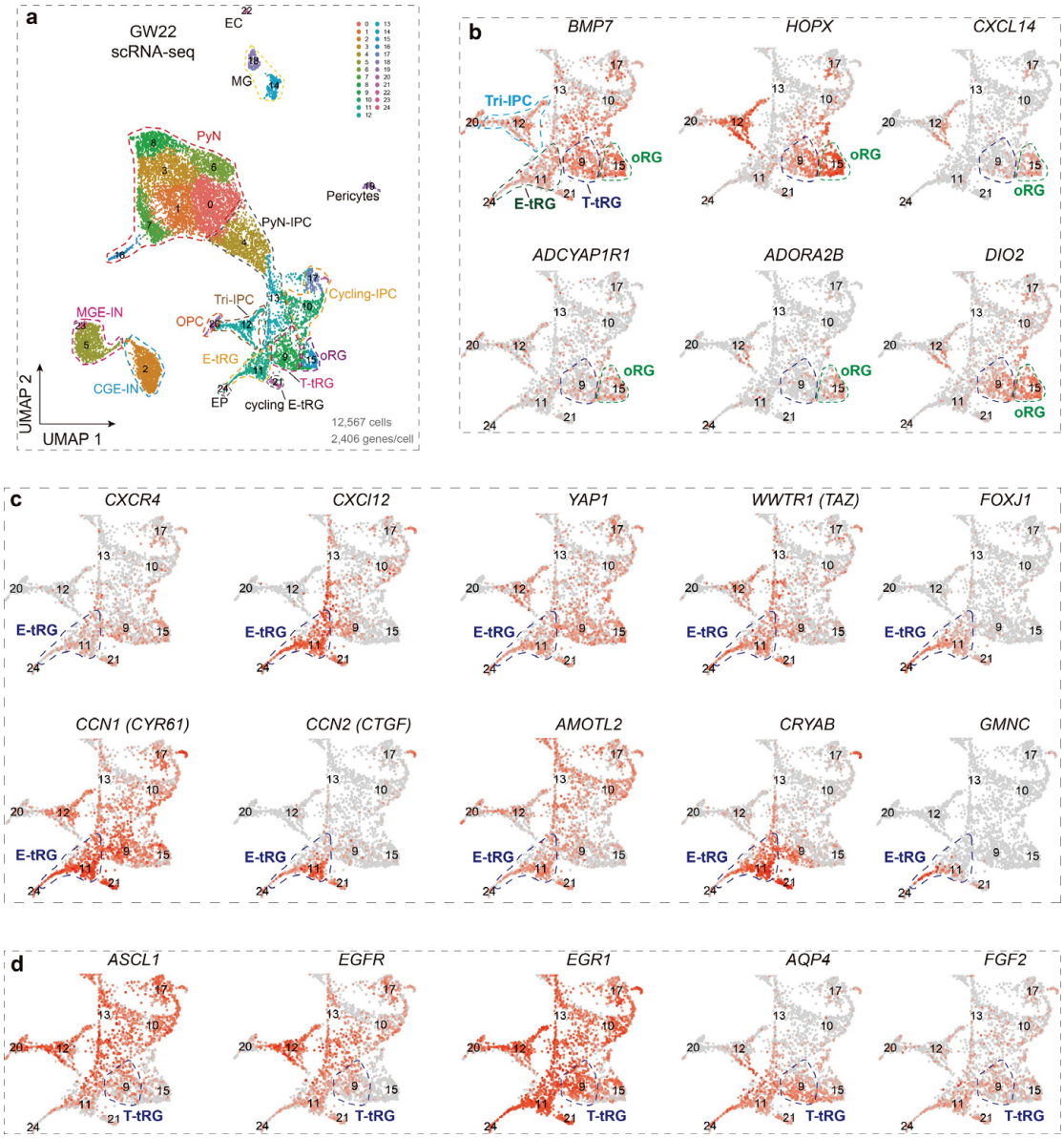

Extended Data Fig. 1 | Expression of cell-type-specific markers in scRNA-Seq data at GW22. a, UMAP of GW22 scRNA-Seq cells colored by cluster (from Fig. 1**a**) [17]. **b-d**, UMAP plots showing gene expression in human cortical progenitors. Note that key components of the cortical PKA signaling, including *ADCYAP1R1, ADORA2B, DIO2*, and *CXCL14*, demonstrate significantly elevated expression levels in oRGs (**b**). FOXJ1 and GMNC (GEMC1) are two master regulators essential for initiating the multiciliation program. Note that the onset of FOXJ1 expression in E-tRGs precedes that of GMNC (**c**). oRG, outer radial glia; E-tRG, ependymal-IPC-generating truncated radial glia, T-tRG, Tri-IPC-generating tRG; EP, ependymal cell; Tri-IPCs, tripotential intermediate progenitor cells; OPC, oligodendrocyte lineage-restricted IPCs; PyN, cortical glutamatergic pyramidal neuron; PyN-IPC, PyN intermediate progenitor cells; CGE-IN, caudal ganglionic eminence interneuron; MGE-IN, medial ganglionic eminence interneuron; EC, endothelial cell; MG, microglia.

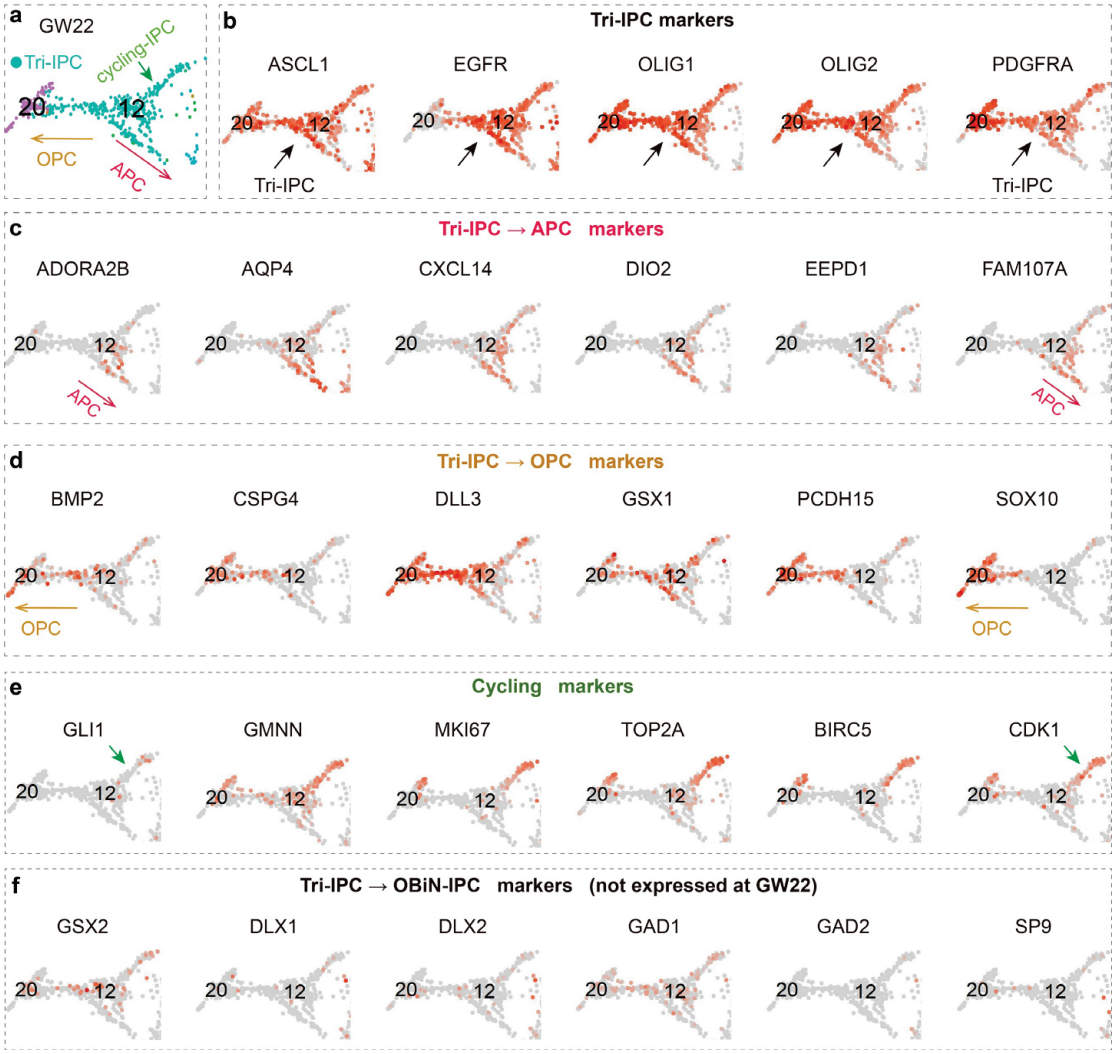

Extended Data Fig. 2 | Cortical T-tRG-derived Tri-IPCs at GW22 do not generate OBIN-IPCs. a-f, While marker genes for cortical Tri-IPCs, APCs, OPCs, and cycling progenitors, are identified (arrows in **a-e**), OBIN-IPC marker genes are not observed in Tri-IPC clusters at GW22 (**f**). APC, astrocyte lineage-restricted IPCs; OBIN-IPC, IPCs for cortically derived olfactory bulb interneuron.

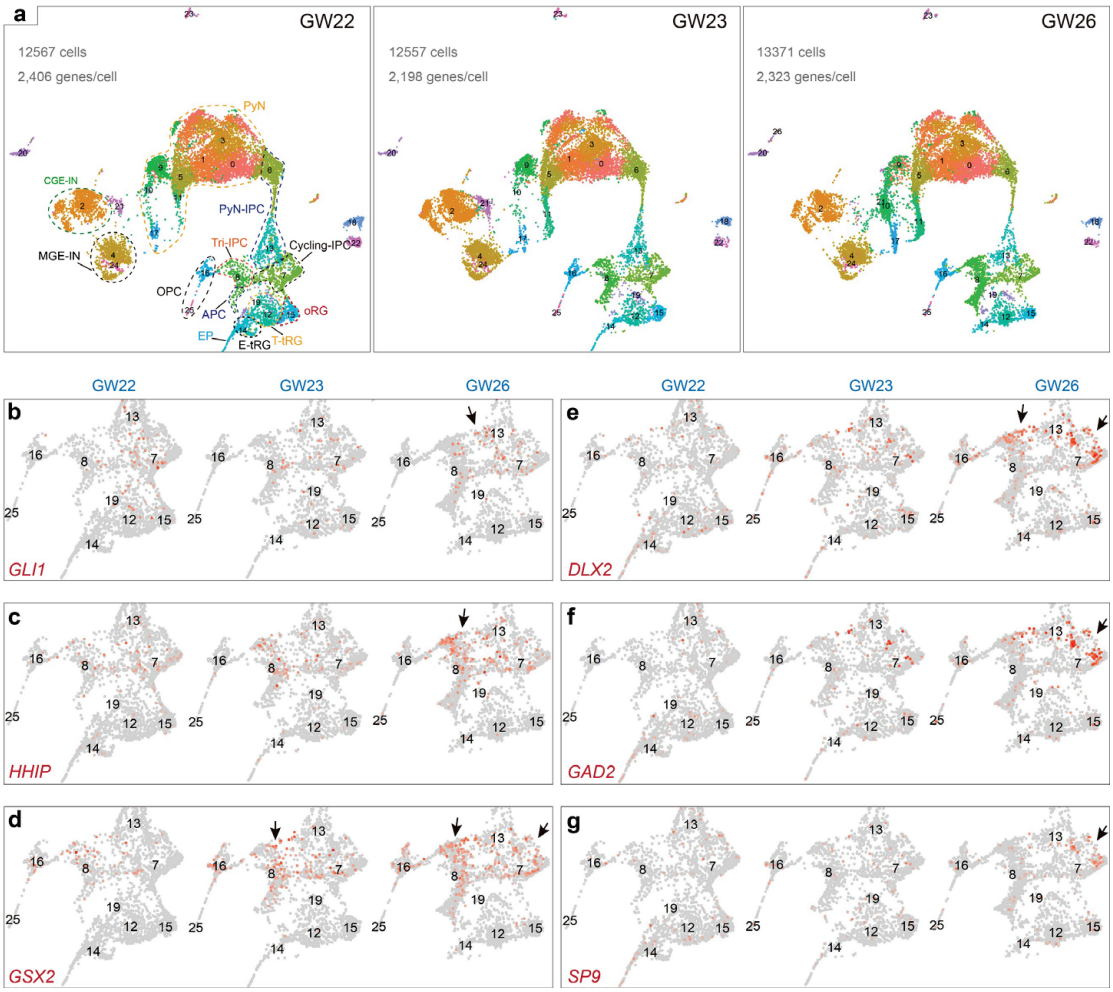

Extended Data Fig. 3 | Cortical T-tRG-derived Tri-IPCs at GW23 and GW26 undergo progressive generating OBIN-IPCs. a, UMAP of GW22, GW23, and GW26 scRNA-Seq cells colored by cluster [17]. **b, c**, *GLI1* and *HHIP* expression levels showing a gradual increase in cortical progenitors from GW22 to GW26 (arrows). **d-f**, Expression of key OBIN-IPC markers, including *GSX2, DLX2, GAD2*, and *SP9*, within Tri-IPC cluster, are observed at GW26 (arrows).

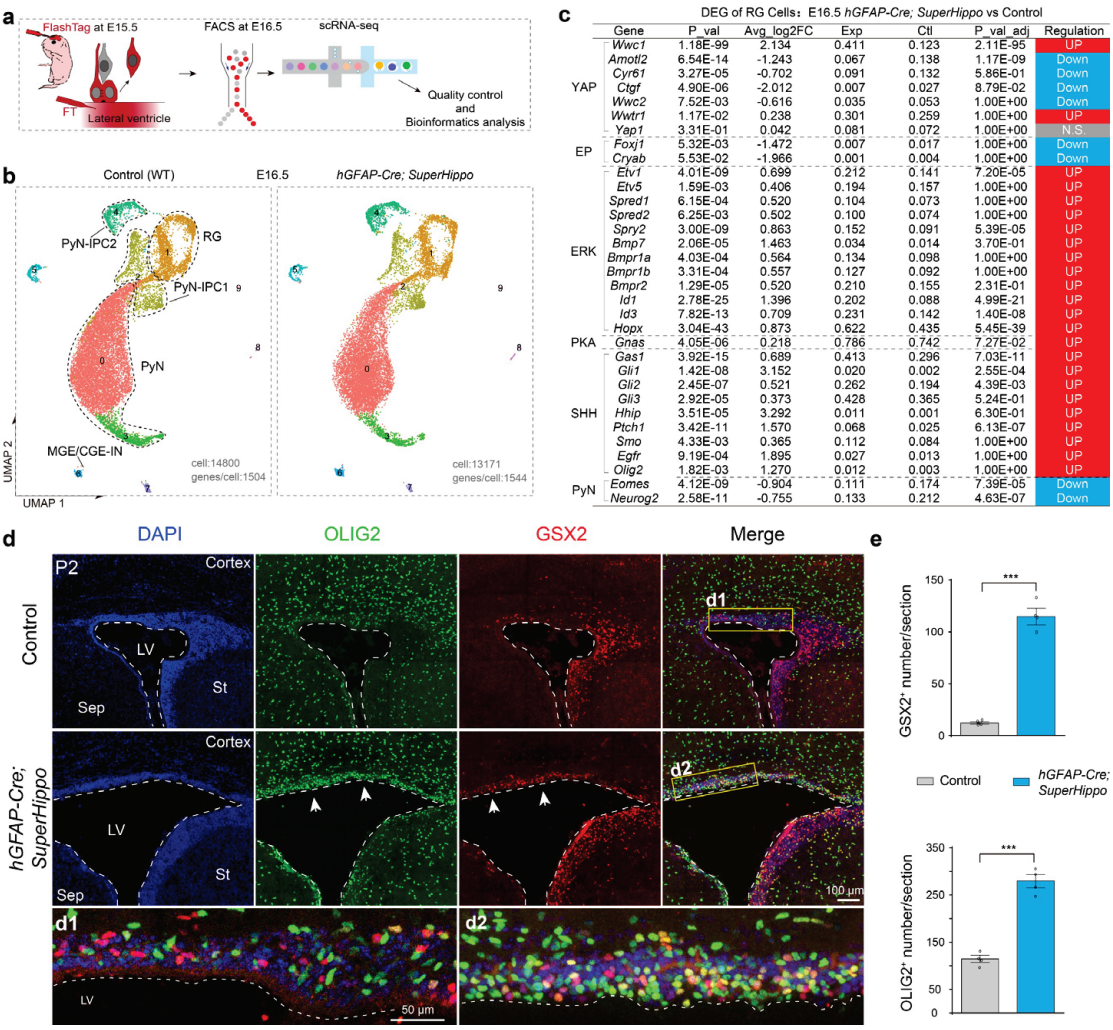

	Gene	P_val	Avg_log2FC	Exp	Ctl	P_val_adj	Regulation
YAP	*Wwc1*	1.18E-99	2.134	0.411	0.123	2.11E-95	UP
	Amotl2	6.54E-14	-1.243	0.067	0.138	1.17E-09	Down
	Cyr61	3.27E-05	-0.702	0.091	0.132	5.86E-01	Down
	Ctgf	4.90E-06	-2.012	0.007	0.027	8.79E-02	Down
	Wwc2	7.52E-03	-0.616	0.035	0.053	1.00E+00	Down
	Wwtr1	1.17E-02	0.238	0.301	0.259	1.00E+00	UP
	Yap1	3.31E-01	0.042	0.081	0.072	1.00E+00	N.S.
EP	*Foxj1*	5.32E-03	-1.472	0.007	0.017	1.00E+00	Down
	Cryab	5.53E-02	-1.966	0.001	0.004	1.00E+00	Down
ERK	*Etv1*	4.01E-09	0.699	0.212	0.141	7.20E-05	UP
	Etv5	1.59E-03	0.406	0.194	0.157	1.00E+00	UP
	Spred1	6.15E-04	0.520	0.104	0.073	1.00E+00	UP
	Spred2	6.25E-03	0.502	0.100	0.074	1.00E+00	UP
	Spry2	3.00E-09	0.863	0.152	0.091	5.39E-05	UP
	Bmp7	2.06E-05	1.463	0.034	0.014	3.70E-01	UP
	Bmpr1a	4.03E-04	0.564	0.134	0.098	1.00E+00	UP
	Bmpr1b	3.31E-04	0.557	0.127	0.092	1.00E+00	UP
	Bmpr2	1.29E-05	0.520	0.210	0.155	2.31E-01	UP
	Id1	2.78E-25	1.396	0.202	0.088	4.99E-21	UP
	Id3	7.82E-13	0.709	0.231	0.142	1.40E-08	UP
	Hopx	3.04E-43	0.873	0.622	0.435	5.45E-39	UP
PKA	*Gnas*	4.05E-06	0.218	0.786	0.742	7.27E-02	UP
SHH	*Gas1*	3.92E-15	0.689	0.413	0.296	7.03E-11	UP
	Gli1	1.42E-08	3.152	0.020	0.002	2.55E-04	UP
	Gli2	2.45E-07	0.521	0.262	0.194	4.39E-03	UP
	Gli3	2.92E-05	0.373	0.428	0.365	5.24E-01	UP
	Hhip	3.51E-05	3.292	0.011	0.001	6.30E-01	UP
	Ptch1	3.42E-11	1.570	0.068	0.025	6.13E-07	UP
	Smo	4.33E-03	0.365	0.112	0.084	1.00E+00	UP
	Egfr	9.19E-04	1.895	0.027	0.013	1.00E+00	UP
	Olig2	1.82E-03	1.270	0.012	0.003	1.00E+00	UP
PyN	*Eomes*	4.12E-09	-0.904	0.111	0.174	7.39E-05	Down
	Neurog2	2.58E-11	-0.755	0.133	0.212	4.63E-07	Down

Extended Data Fig. 4 | A significant upregulation of ERK, PKA, and SHH pathway activities in cortical RGs following YAP signaling ablation. a, Strategy for labeling (via lateral ventricle injection of FlashTag-CellTrace Yellow at E15.5) and enriching cortical progenitor cells from two littermate controls (wild type, WT) brains and two *hGFAP-Cre; SuperHippo* brains at E16.5 and scRNA-Seq analysis. **b**, Annotation of cortical cell clusters. **c**, scRNA-Seq analysis revealed differentially expressed genes (DEG) in E16.5 cortical RGs (cluster 1 in **a**) of *hGFAP-Cre; SuperHippo* mice relatively to WT controls. **d, e,** Immunostaining reveals disruption of the cortical ventricular surface and increase in GSX2- and OLIG2-expressing progenitors in the cortical VZ/SVZ of *hGFAP-Cre; SuperHippo* mice at P2.

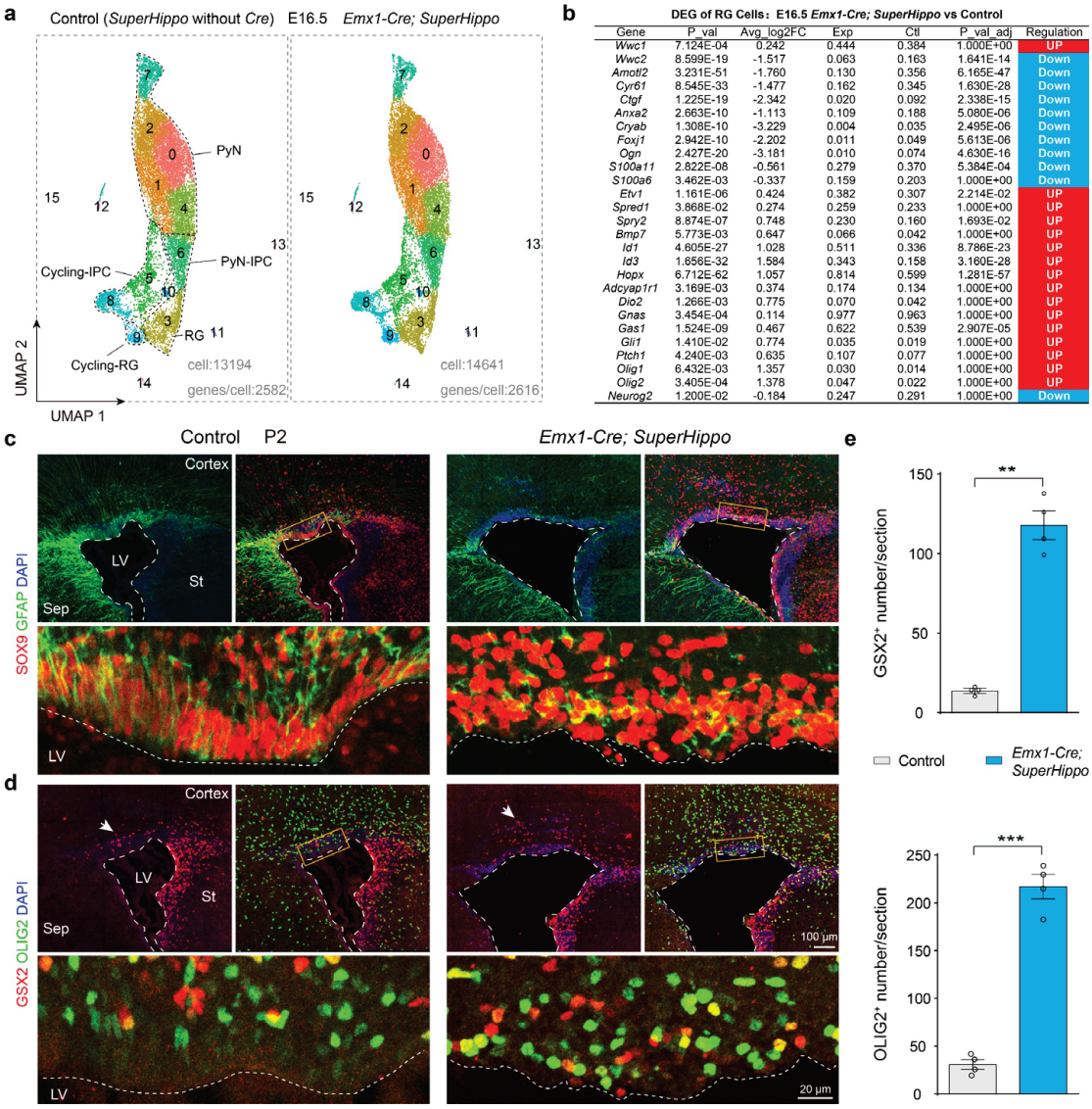

DEG of RG Cells: E16.5 *Emx1-Cre; SuperHippo* vs Control

Gene	P_val	Avg_log2FC	Exp	Ctl	P_val_adj	Regulation
Wwc1	7.124E-04	0.242	0.444	0.384	1.000E+00	UP
Wwc2	8.599E-19	-1.517	0.063	0.163	1.641E-14	Down
Amotl2	3.231E-51	-1.760	0.130	0.356	6.165E-47	Down
Cyr61	8.545E-33	-1.477	0.162	0.345	1.630E-28	Down
Ctgf	1.225E-19	-2.342	0.020	0.092	2.338E-15	Down
Anxa2	2.663E-10	-1.113	0.109	0.188	5.080E-06	Down
Cryab	1.308E-10	-3.229	0.004	0.035	2.495E-06	Down
Foxj1	2.942E-10	-2.202	0.011	0.049	5.613E-06	Down
Ogn	2.427E-20	-3.181	0.010	0.074	4.630E-16	Down
S100a11	2.822E-08	-0.561	0.279	0.370	5.384E-04	Down
S100a6	3.462E-03	-0.337	0.159	0.203	1.000E+00	Down
Etv1	1.161E-06	0.424	0.382	0.307	2.214E-02	UP
Spred1	3.868E-02	0.274	0.259	0.233	1.000E+00	UP
Spry2	8.874E-07	0.748	0.230	0.160	1.693E-02	UP
Bmp7	5.773E-03	0.647	0.066	0.042	1.000E+00	UP
Id1	4.605E-27	1.028	0.511	0.336	8.786E-23	UP
Id3	1.656E-32	1.584	0.343	0.158	3.160E-28	UP
Hopx	6.712E-62	1.057	0.814	0.599	1.281E-57	UP
Adcyap1r1	3.169E-03	0.374	0.174	0.134	1.000E+00	UP
Dio2	1.266E-03	0.775	0.070	0.042	1.000E+00	UP
Gnas	3.454E-04	0.114	0.977	0.963	1.000E+00	UP
Gas1	1.524E-09	0.467	0.622	0.539	2.907E-05	UP
Gli1	1.410E-02	0.774	0.035	0.019	1.000E+00	UP
Ptch1	4.240E-03	0.635	0.107	0.077	1.000E+00	UP
Olig1	6.432E-03	1.357	0.030	0.014	1.000E+00	UP
Olig2	3.405E-04	1.378	0.047	0.022	1.000E+00	UP
Neurog2	1.200E-02	-0.184	0.247	0.291	1.000E+00	Down

Extended Data Fig. 5 | YAP signaling represses ERK, PKA, and SHH pathway activities in cortical RGs. a, UMAP of scRNA cells colored by cluster. **b**, scRNA-Seq analysis revealed differentially expressed genes (DEG) in E16.5 cortical RGs (cluster 3 in **a**) of *Emx1-Cre; SuperHippo* mice relatively to controls (*SuperHippo* mice without *Emx1-Cre*). **c-e**. At P2, immunostaining reveals disruption of the cortical ventricular surface and the loss of apical SOX9- and GFAP-expressing immature ependymal cells in the *Emx1-Cre; SuperHippo* cortex. Consistent with the elevated SHH signaling activity in cortical RGs, quantitative analysis demonstrated a significant expansion of GSX2- and OLIG2-expressing progenitor in the cortical VZ/SVZ of *Emx1-Cre; SuperHippo* mice.

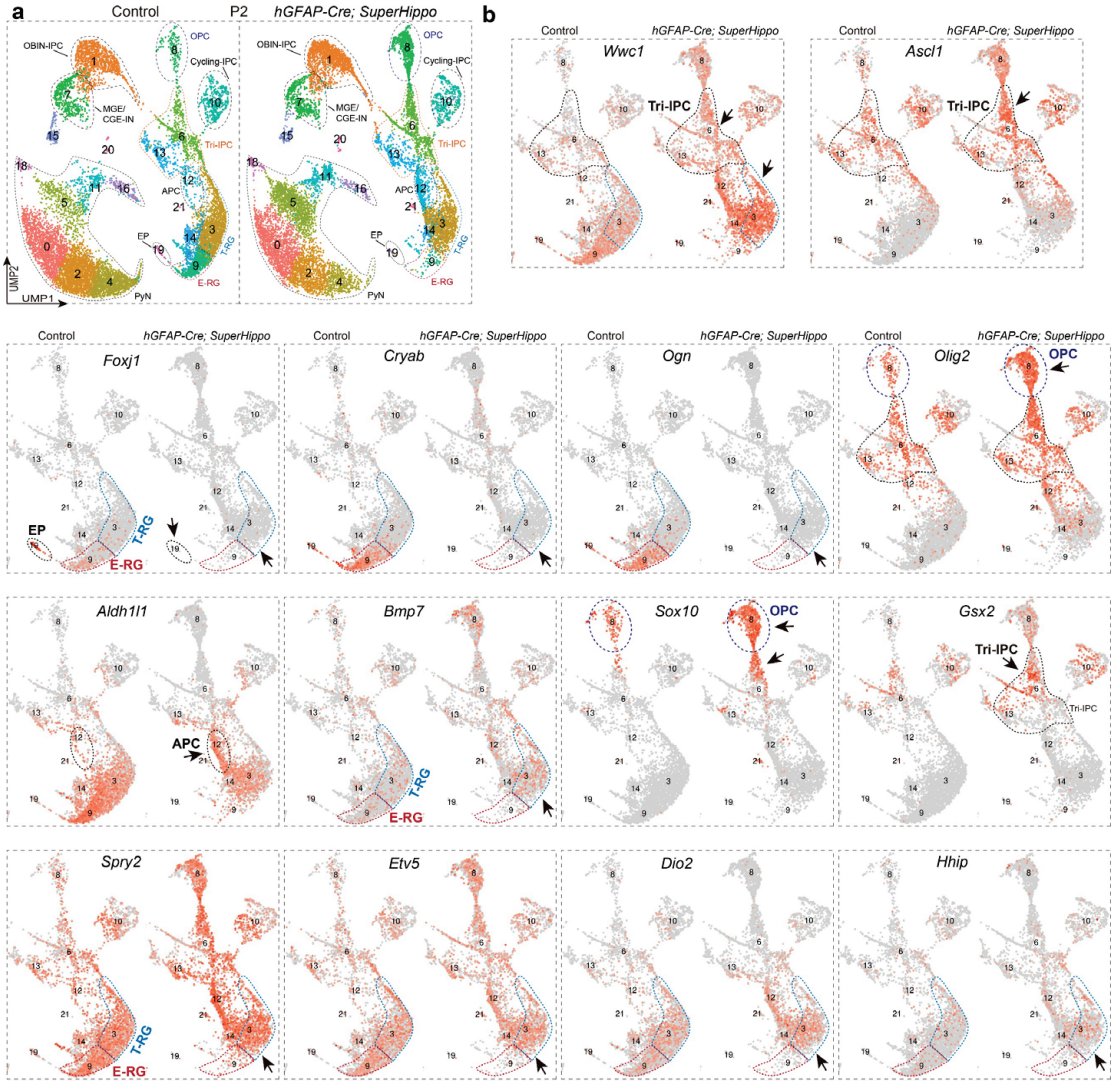

Extended Data Fig. 6 | Loss of YAP signaling results in the depletion of cortical E-RGs and ependymal cells. a, UMAP of scRNA cells colored by cluster (from Figure 2**b**). **b**, UMAP plots showing *Wwc1* gene expression was increased in *hGFAP-Cre; SuperHippo* (*Wwc1*-derived *SuperHippo* minigene) mice at P2. Note that loss of YAP signaling results in the depletion of cortical E-RGs and the loss of early ependymal marker gene expression in cortical T-RGs, including *Foxj1*, *Cryab*, and *Ogn*. In contrast, there is the upregulation of genes related to Tri-IPCs (*Ascl1* and *Olig2*), APCs (*Aldh1l1*), OPCs (*Sox10*), OBIN-IPCs (*Gsx2*), ERK signaling (*Bmp7, Spry2*, and *Etv5*), PKA signaling (*Dio2*), and SHH signaling (*Hhip*).

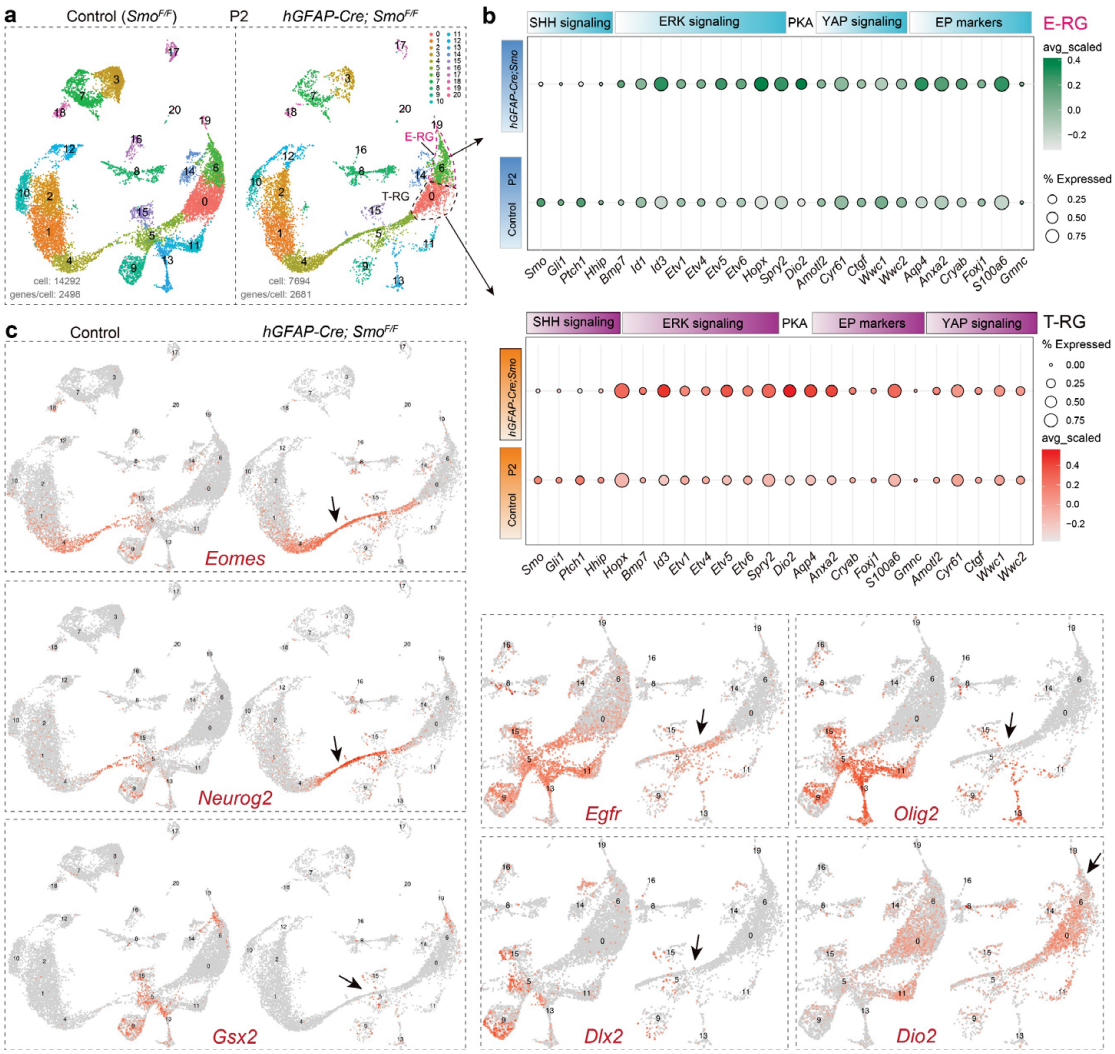

Extended Data Fig. 7 | SHH-SMO signaling inhibits PKA, ERK, and YAP signaling pathways. a, UMAP of scRNA cells colored by cluster. **b**, Bubble plot showing differentially expressed genes (DEG) in cortical E-RGs and T-RGs in *control* (*Smo*$^{F/F}$) and *hGFAP-Cre; Smo*$^{F/F}$ mice at P2. **c**, UMAP plots showing differentially expressed genes in the cortex of *control* (*Smo*$^{F/F}$) and *hGFAP-Cre; Smo*$^{F/F}$ mice at P2. In the absence of *Smo* function, *Eomes, Neurog2* and *Dio2* expression were increased in cortical RGs and/or progenitors, whereas *Gsx2*, *Egfr*, *Olig2*, and *Dlx2* expression were significantly reduced.

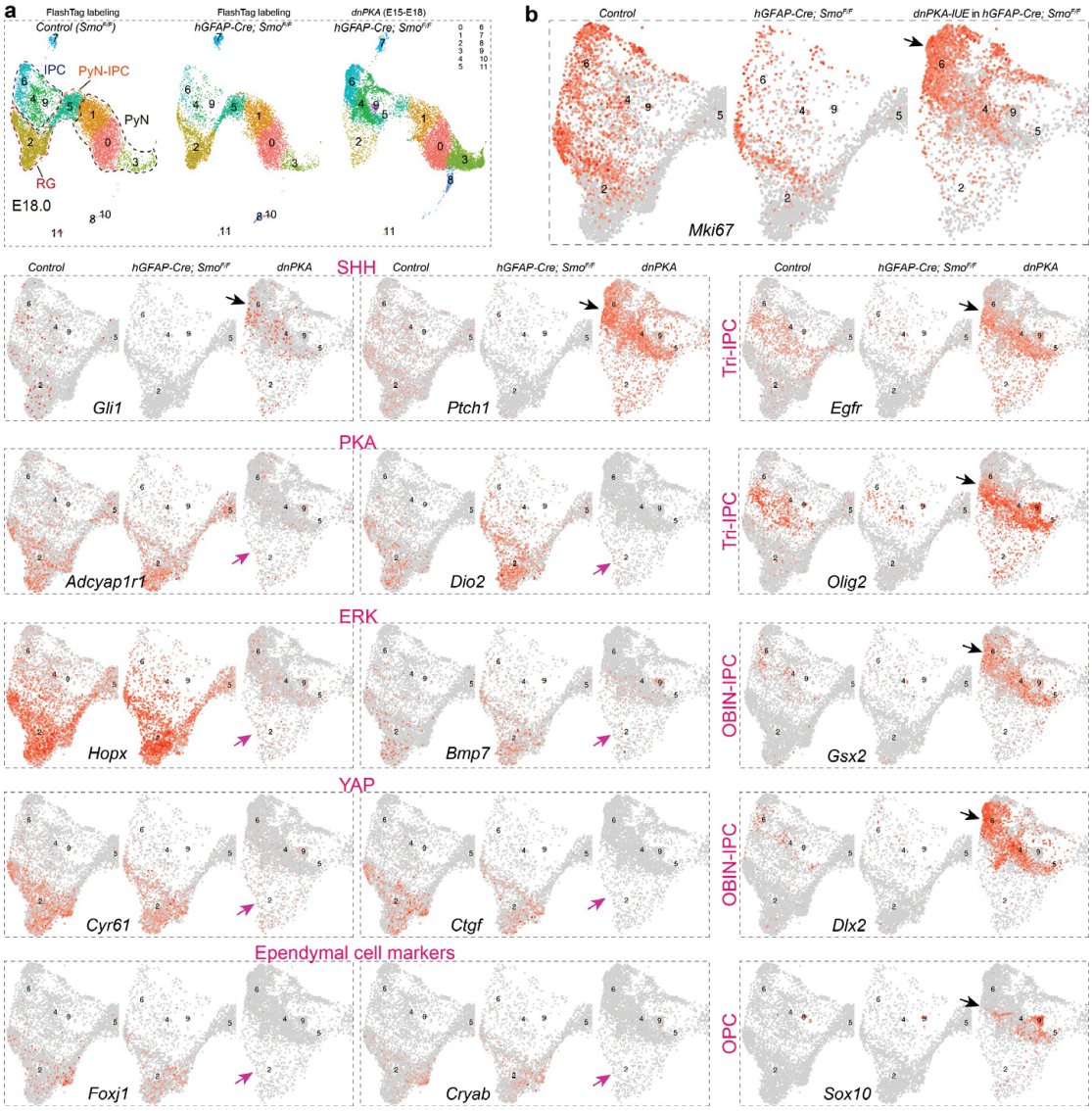

Extended Data Fig. 8 | PKA signaling strongly inhibits SHH-SMO signaling. a, UMAP of scRNA cells colored by cluster (from Figure 3**b**). **b**, UMAP plots showing individual gene expression in the cortex of *Smo*$^{F/F}$, *hGFAP-Cre; Smo*$^{F/F}$, and *hGFAP-Cre; Smo*$^{F/F}$ mouse with IUE of *dnPKA* at E18.0. The complete loss of PKA in cortical RGs results in a significant increase in SHH signaling (*Gli1* and *Ptch1*), even in the absence of *Smo* function. This is accompanied by the depletion of PKA (*Adcyal1r1* and *Dio2*), ERK (*Hopx* and *Bmp7*), and YAP (*Cyr61* and *Ctgf*) signaling, as well as the loss of early ependymal marker gene (*Foxj1* and *Cryab*) expression. In contrast, there is a significant upregulation of genes associated with Tri-IPCs (*Egfr* and *Olig2*), OBIN-IPCs (*Gsx2* and *Dlx2*), and OPCs (*Sox10*).

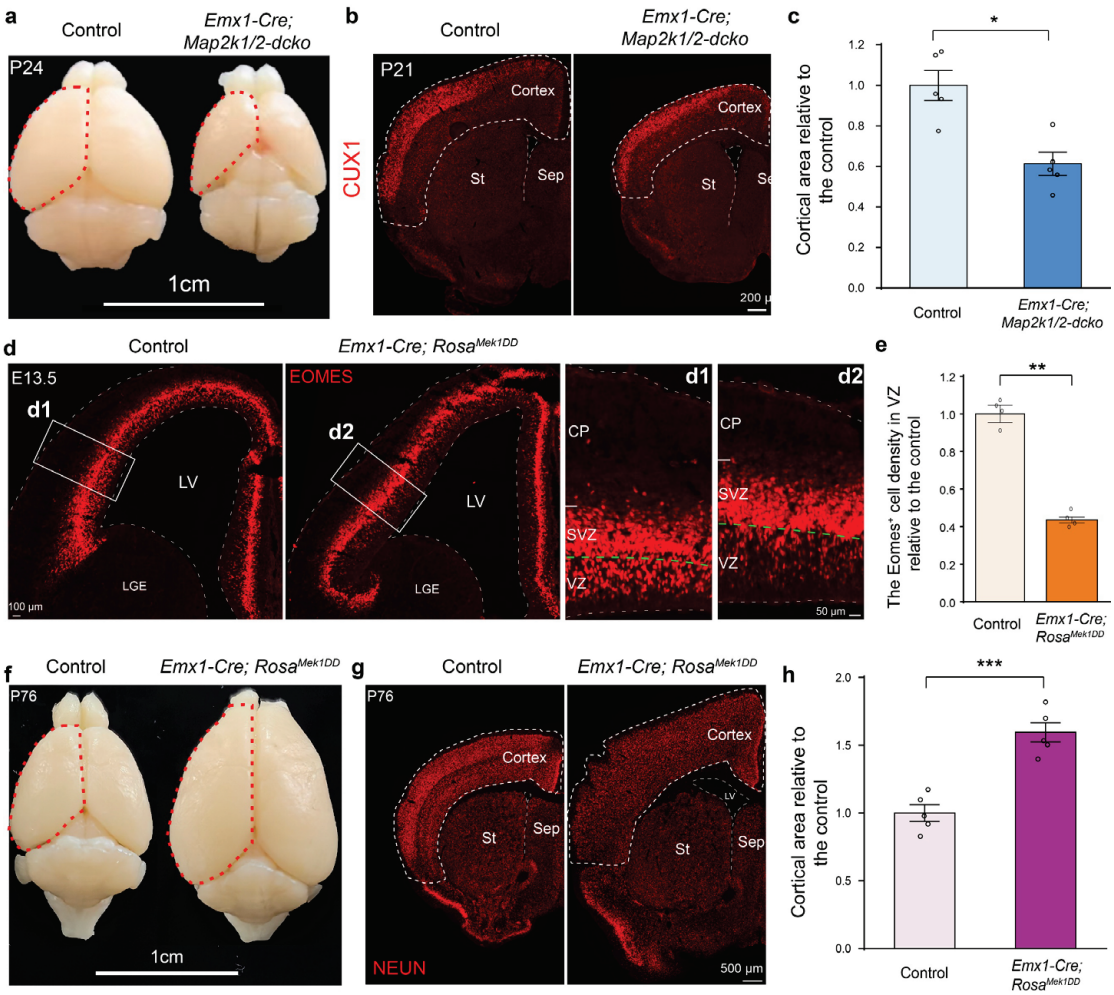

Extended Data Fig. 9 | Loss and gain of ERK function from E10.5 cortical RGs result in pronounced microcephaly and macrocephaly, respectively. a, Whole mount images of control and *Emx1-Cre; Map2k1/2-dcko* brains. **b**, Immunostaining for CUX1 revealed fewer upper-layer PyNs and a smaller cortical area in *Emx1-Cre; Map2k1/2-dcko* cortices. **c**, Quantification of the cortical area within the cortical plate in *control* and *Emx1-Cre; Map2k1/2-dcko* mice. **d, e,** Immunostaining for EOMES, a marker of PyN-IPCs, revealed fewer EOMES-expressing cells in the VZ of *Emx1-Cre; Rosa*^{MEK1DD} mice at E13.5, suggesting an expansion of cortical RGs and restricted neuronal differentiation following enhanced ERK signaling. LGE, Lateral ganglionic eminence. **f,** Whole mount images of control and *Emx1-Cre; Rosa*^{MEK1DD} brains at P76. **g**, Immunostaining for NEUN, a marker of neurons. **h**, Quantification revealed a larger cortical area in *Emx1-Cre; Rosa*^{MEK1DD} mice at P76.

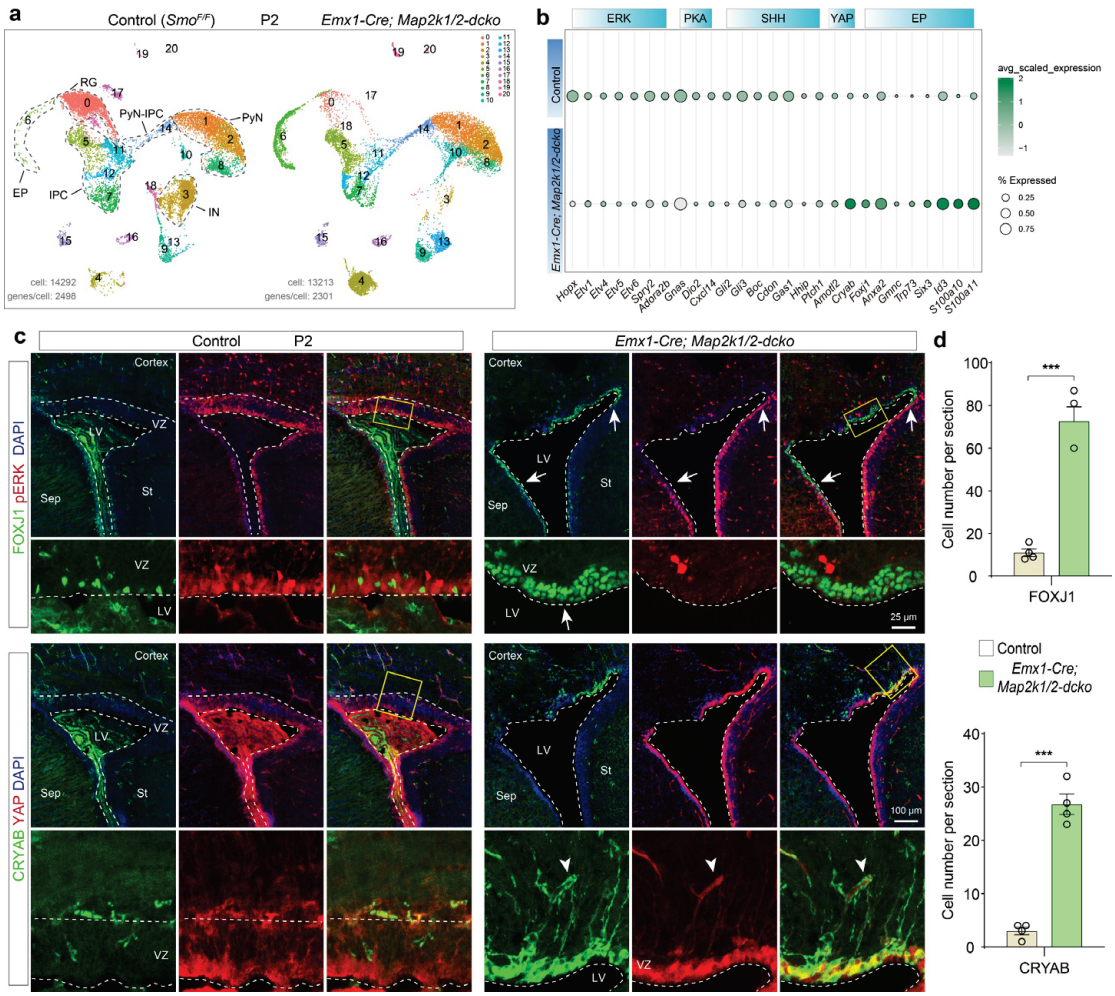

Extended Data Fig. 10 | Loss of ERK signaling leads to downregulated PKA and SHH signaling, and increased YAP signaling. a, UMAP showing annotated cell clusters based on scRNA-Seq analysis of P2 control and *Emx1-cre; Map2k1/2 dcko* cortical cells. **b**, Bubble plot showing the expression of selected ERK, PKA, SHH, and YAP signaling response genes, as well as early cortical ependymal cell genes, in cortical RGs (cluster 0 in **a**) of *Emx1-Cre; Map2k1/2-dcko* mice compared to littermate controls at P2. **c**, FOXJ1- and CRYAB-expressing cells are significantly increased in the cortical VZ of *Emx1-Cre; Map2k1/2-dcko* mice, compared to the few FOXJ1- and CRYAB-expressing cells observed in control mice at P2. Note that, in blood vessels, endothelial cells and vascular smooth muscle cells also expressed CRYAB and YAP/TAZ (arrowheads).

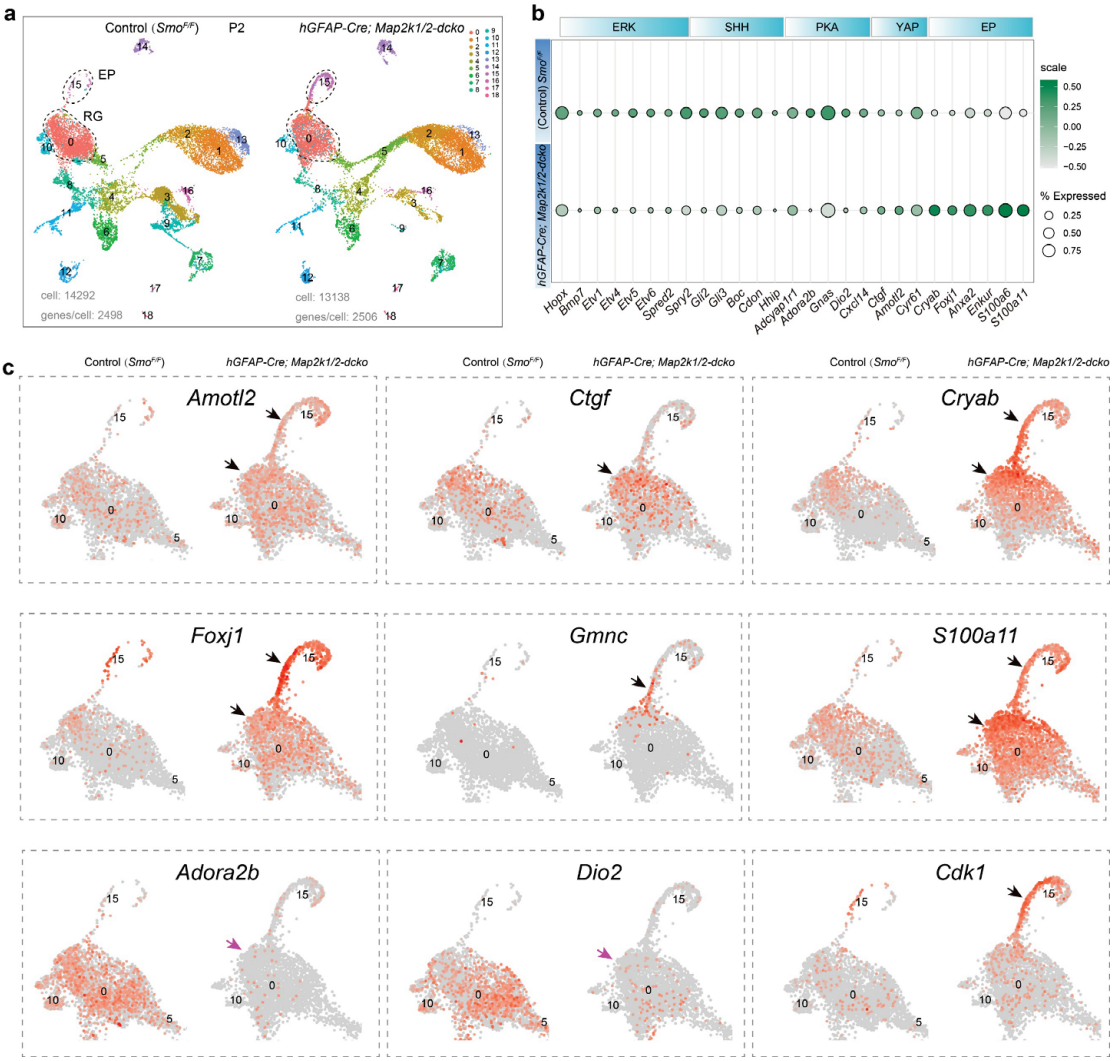

Extended Data Fig. 11 | ERK signaling sustains PKA signaling and inhibits YAP signaling in cortical RGs. a, UMAP showing annotated cell clusters based on scRNA-Seq analysis of P2 control and *hGFAP-Ce; Map2k1/2 dcko* cortical cells. **b**, Bubble plot showing differentially expressed genes in cortical RGs (cluster 0 in **a**) of *hGFAP-Cre; Map2k1/2-dcko* mice compared to controls at P2. **c**, UMAP plots showing differentially expressed genes of YAP and PKA signaling pathway and early ependymal cell marker genes.